2008

Advancement and optimization of an electrospray injection based in-vacuum patterning system for macromolecular materials

Andreas Stark
University of South Florida

Advancement and Optimization of an Electrospray Injection Based In-Vacuum Patterning System for Macromolecular Materials

by

Andreas Stark

A thesis submitted in partial fulfillment
of the requirements for the degree of
Master of Science in Electrical Engineering
Department of Electrical Engineering
College of Engineering
University of South Florida

Major Professor: Rudy Schlaf, Ph.D.
Matthias Batzill, Ph.D.
Jing Wang, Ph.D.

Date of Approval:
May 20, 2008

Keywords: electrospray ionization, ion focussing, ion funnel, cytochrome c, faraday cup

ACKNOWLEDGEMENTS

I would like to thank Dr. Rudy Schlaf for the opportunity of writing this thesis, my committee members Dr. Matthias Batzill and Dr. Jing Wang for their support and time, Dr. Mark Anthony and Dr. Martin Beerbom for their support, Florian Kaiser and Matthew Holland for their help, the USF machine shop for its excellent work, all group members and EE Department staff for their help and support and Chuck from the Coffee shop for the first wrapping foil. I also would like to thank Romina Wiedmann for her great support and lending me her ears for my problems and my family who made it all possible.

TABLE OF CONTENTS

LIST OF FIGURES

Advancement and Optimization of an Electrospray Injection Based In-Vacuum Patterning System for Macromolecular Materials

Andreas Stark

ABSTRACT

Electrospray ionization is a technique widely used in mass spectrometry. Almost every material, specifically large molecules like proteins or polymers can be ionized directly out of solution. During the ionization process molecules are not fragmented. In this work a prototype apparatus for creating three-dimensional patterns in a ultra high vacuum environment using an electrospray ion source was optimized for higher ion currents hence deposition rate by improving the core component of the apparatus, an electrodynamic ion funnel. The major improvements are a redesigned heated vacuum inlet, modified gas flow inside the ion funnel because of sealing the ion funnel against perpendicular gas flow and a better measurement setup for the transmitted current. The transmission of the ion funnel was improved from 25% to 82% resulting in ion currents of up to 7nA (500pA before advancements) focused through the ion funnel. At this rate an area of 1 cm^2 can be coated with a molecular monolayer of Cytochrome C in 64 minutes.

1 INTRODUCTION

Many applications for a controlled assembly of macro-molecular materials to complex 3D structures exist. These are for example the production of electronic devices and biomedical sensors. But the main problem is to control the exact and three-dimensional deposition of those macro-molecules within the accuracy of nanometers in a high vacuum environment. The vacuum is necessary as few impurity atoms can affect the functionality of nanometer-size devices. Also not exact deposition due to limited accuracy can affect the desired functionality of a device.

The approach of Dr. Rudy Schlaf's research group to produce 3D structures of macro-molecules is to generate a beam of ionized macro-molecules (ion beam) by an electrospray ion source (see sections 1.2 and 2.2) in a vacuum chamber and use electrical and magnetic fields to control this beam similar to the electron beam in a TV set. A prototype of a 3D patterning device for macro-molecular materials ("MoleculeWriter", [9]) is currently being developed. Up to now there exists no method of generation an ion beam without destroying macro-molecular materials within a vacuum environment. Hence there are three main problems to solve:

- Generate a beam of ionized macro-molecules and inject it into a vacuum chamber
- Minimize losses between ion source and target
- Control the ion beam with high accuracy

1.1 Objective of this thesis

In the work done during this thesis the main focus was on solving the first two problems. To generate 3D structures consisting of macro-molecules economically the main cost factor is the production time per device. The main limiting factor is the deposition rate. The higher the deposition rate, the faster macro-molecules can be deposited and more 3D structures can be produced per time. Only with a high ion current (ions per time) a high deposition rate can be achieved. So there are two processes to be optimized:

- Output from the ion source
- Loss between ion source and deposition target

To achieve high performance, high output and low loss is needed. A high output from the ion source leads to a high ion density within the beam. But this is contrary to a high performance because all the ions have the same polarity, they repel each other and so the beam is spread out and loss increases.

During the work for this thesis the existing prototype system was characterized to gain better understanding of the electrospray process and the loss sources. Thereafter the main focus was on running a redesigned prototype system, specifically a redesigned ion funnel to improve the ion current into the second vacuum chamber of the system and reach economical deposition times.

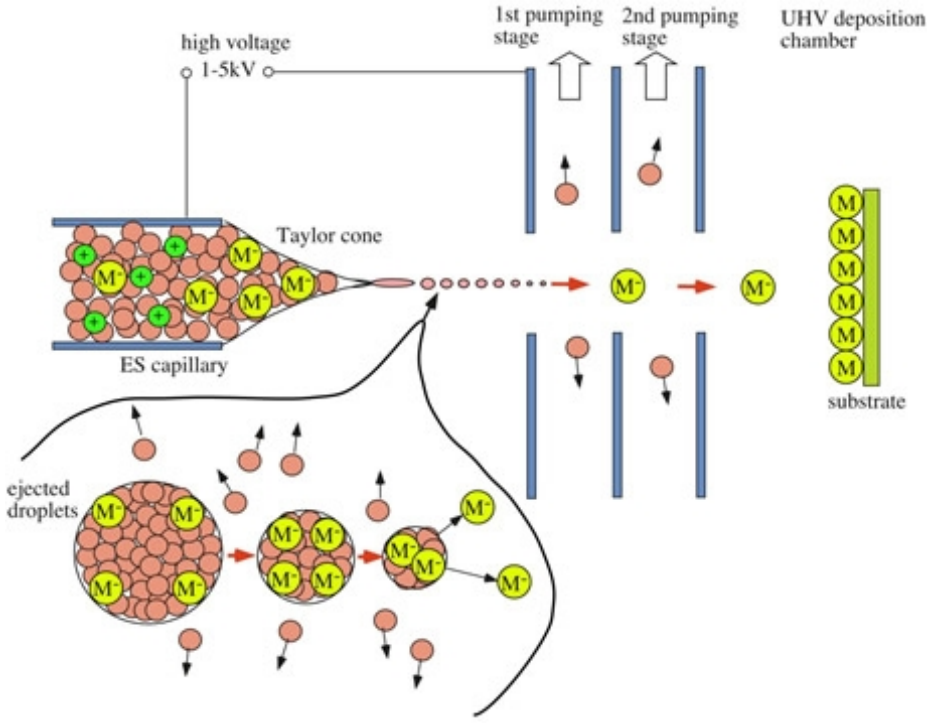

a) strong electric field extracts droplets from Taylor cone containing solute ions M^-; most counterions $\oplus$ remain in capillary

b) solvent evaporates, droplets shrink, charge density increases

c) solute ions are ejected from the droplets; solvent is removed in pumping stages

d) solute molecules enter the preparation chamber and form thin film

Figure 1.1: Electrospray injection process, obtained from [8].

1.2 Electrospray ionization

Usually macro-molecules, specifically biomolecules like peptides, proteins or DNA (deoxyribonucleic acid) are only available in solution. A technique known from mass spectrometry to create a beam of ionized macro-molecules, is electrospray (ES) ionization. Electrospray ionization is based on the work of Dole 1968 [5] and was established by Fenn 1984 [35] (Nobel Prize in Chemistry 2002).

Figure 1.1 shows the electrospray ionization and injection process: The desired macro-molecules are pumped through the electrospray capillary. Surface tension of the solution and the applied electric field between capillary and vacuum inlet lead to the formation of the "Taylor cone" (detailed explanation in section 2.2), where positive and negative ions are separated. At the tip of the Taylor cone mainly uniform droplets consisting of uncharged solvent molecules and ionized macro-molecules are emitted due to increasing instability with increasing distance from the capillary end.

During the flight uncharged solvent evaporates and droplets get smaller and charge density on the surface of the droplet increases. After shrinking to a certain radius (Rayleigh limit [23]) the droplet gets instable because of the high charge density and disintegrate into smaller droplets as the Coulomb repulsion forces exceed the surface tension that hold the droplets together.

The small droplets and ions are then guided by the electric field and air flow into the vacuum chamber.

1.3 MoleculeWriter prototype

Prof. Dr. Schlaf's group has designed a prototype apparatus to realize the objective of patterning 3D structures of macro-molecules. The "MoleculeWriter" [8] prototype is described in detail in chapter 3.

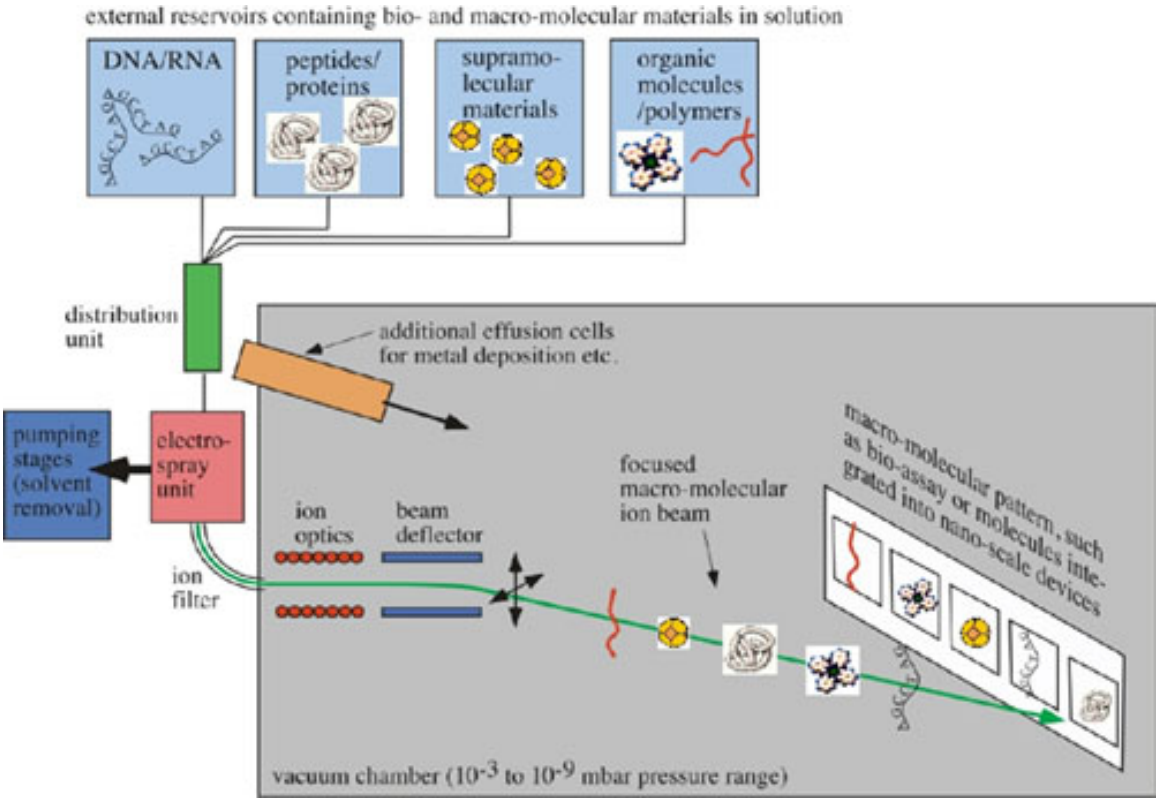

Figure 1.2: Production of 3D structures with the MoleculeWriter, obtained from [9]. Solutions containing macro-molecules are ionized through the electrospray (ES) device. The resulting beam of ionized macro-molecules is focused by ion optics and mass filtered to extract the desired molecules. Before hitting a substrate surface, the beam can be deflected similar to the electron beam in a TV set to produce 3D patterns like nano-composite layers and small coated areas on sensor arrays.

Figure 1.2 shows the concept of the MoleculeWriter. A distribution unit selects a solution containing the desired macro-molecules. This solution is pumped into the *electrospray unit*, where a beam of ionized, gas-phase macro-molecules is created as described in section 1.2. Until this point the process takes place at atmospheric pressure. Now the beam passes the *vacuum interface* that can be a capillary or orifice. *Differential pumping stages* remove remaining solvent from the macro-molecules and reduce the pressure stepwise from atmospheric pressure to 10^{-3} till 10^{-9} mBar ($\frac{1}{1 \text{ million}}$ till $\frac{1}{1 \text{ trillion}}$ of atmospheric pressure).

The beam is focused by an *"ion funnel"* (see section 3.4) to minimize losses due to the natural spreading out of the beam. Our ion funnel consists of a stack of metal plates (lenses) with concentric holes of decreasing diameter, separated by spacers. A combination of DC (constant voltage) and RF (high frequency) signal is applied to the lenses. The electric RF field created by this signal focuses the ion beam.

After being focused the ion beam is mass-filtered and can be deflected by the beam deflector to control the deposition position on the substrate surface. This allows to create 3D patterns of macro-molecules such as bio-assays[1] and molecules integrated into nano-scale devices.

[1] Device to determine the strength or biological activity of a substance, such as a drug or hormone, by comparing its effects with those of a standard preparation on a culture of living cells or a test organism. (Wikipedia)

1.4 Experimental steps

A series of experimental steps and simulations was made to analyze and minimize losses at the vacuum interface and the ion funnel. All the experimental steps are fully described in chapters 4 to 6 and the results are discussed. These have been:

- Characterizing the existing prototype and identifying the main loss sources
- Redesigning the prototype system together with all other group members [2]
- Commissioning the new prototype design
- Optimizing the electrospray and ion funnel parameters to reach and exceed results obtained from other research with similar designs

[2]Prof. Dr. Rudy Schlaf, Dr. Mark Anthony, Dr. Martin Beerbom, Florian Kaiser, Matthew Holland

2 ELECTROSPRAY IONIZATION

2.1 Other ionization techniques

There is an alphabet of ionization techniques, but not all of them are useful for the purpose to create 3D patterns of large molecules without destroying them. The desired ionization technique should also provide a high ion current, so that the production of patterns can be accomplished in a shorter time. It should also be able to ionize a broad spectrum of inorganic and organic materials, specifically biomolecules which are usually available only in solution.

Most of the ionization techniques are known from mass spectrometry where the molecular composition of a sample or macromolecules is analyzed. These are electron ionization (EI), chemical ionization (CI), atmospheric pressure chemical ionization (APCI), fast atom bombardment (FAB), field desorption (FD), matrix-assisted laser desorption/ionization (MALDI), atmospheric pressure photoionization (APPI), electrospray ionization (ESI), desorption electrospray ionization (DESI), glow discharge (GD), inductively coupled plasma (ICP), microwave induced plasma (MIP),

thermospray ionization (TS), direct analysis in real time (DART) and laser diode thermal desorption (LDTD).

Most of them are not useful for our purpose because they require either gas phase or solid state molecules or fragment the molecules during the ionization process. Electrospray has emerged as the best ionization technique for biomolecules in a solution. It has a high efficiency and almost no fragmentation occurs.

2.2 Electrospray

John B. Fenn was awarded the 2002 Nobel price in chemistry for his work on the electrospray ionization technique. He found out during his work that was published in 1984 [35] that using electrospray ionization there is "no evidence of any fragmentation or decomposition of either solvent or solute species". Solute in this case means the macromolecule in solution (= solvent) that is ionized during the electrospray process. In [35] he also states that "the solute ions [...] always appear singly in any clusters", so the macromolecules are transformed into single ions. But Fenn also assumed "possible condensation during the free-jet expansion" in the vacuum chamber, a problem that also occurred during the work for this thesis.

The electrospray ionization process starts with macromolecules beeing ionized in a solution. Then the solution is pumped through a metal

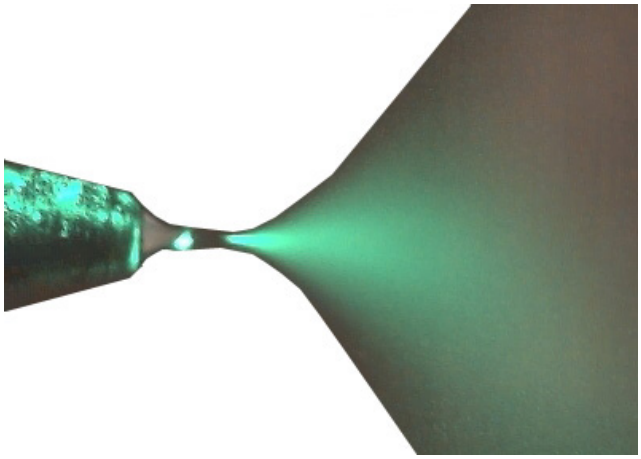

Figure 2.1: Electrospray: A high voltage is applied to the ES needle on the left while pumping a solution of macromolecules through it. At the tip of the Taylor cone a beam of ionized droplets is emitted. Coulomb repulsion force and the electric field widen up the beam to the so called "plume".

capillary (ES needle). Depending on the solvent and the macromolecule either the positive ion mode, where a positive voltage is applied to the ES needle, or the negative ion mode, where a negative voltage is applied, are possible. In this case only the negative ion mode is explained, the positive ion mode is similar, just with opposite charges and voltages.

With a high negative voltage applied to the ES needle the cations (positively charged) in the solution migrate towards the metal wall of the needle and the anions (negatively charged) migrate away from it towards the counter electrode , in this case a metal capillary or orifice at the vacuum chamber entrance. The electric field strength at the needle tip with a planar counter-electrode can be approximated as [12, 17, 21]:

$$E_{needle} = \frac{2V_{needle}}{r_{needle} \ln\left(4d/r_{needle}\right)} \tag{2.1}$$

where V_{needle} is the applied voltage, r_{needle} is the outer radius of the needle and d is the distance between needle tip and counter-electrode. A typical value for E_{needle} for a successful electrospray is $10^6 - 10^7 \frac{V}{m}$ [12, 21]. If the electric field is strong enough, the force on the anions from the electric field is counterbalanced by the surface tension of the solution forming a cone of liquid, called "Taylor cone" [31] at the needle end.

Using a modified [30, 33] form of the Hendricks equation [21] the electrospray current i_{es} can be approximated as:

$$i_{es} = H\nu_f^{\nu}\sigma_S^n E_c^{\varepsilon} \tag{2.2}$$

where H is a constant depending on the surface tension and the dielectric constant of the solvent, ν_f is the flow-rate, σ_S is the specific conductivity and E_c is the electric field from equation 2.1. Experimental work [29, 30] showed that the exponents ν, n and ε can be approximated with those predicted in the Hendricks equation. Fernandez de la Mora and Loscertales[1] determined in their case a current proportional to the square root of electrical conductivity ($n = 1/2$) and flow-rate ($\nu = 1/2$). As a general statement it can be said that i_{es} increases if the conductivity of the solution increases or if the flow-rate is raised [32, 33].

At the tip of the Taylor cone a "jet" of liquid emerges. If the charge density inside this "jet" is too high, it breaks up into droplets. This break-

[1] obtained from [3]

up increases the surface area per charge density and so a stable condition is reestablished. The droplet size increases with decreasing conductivity and in proportion to $(flow - rate)^{2/3}$ [6]. To produce small droplets a small flow-rate and a high conductivity is needed.

The resulting fine spray of droplets of the same polarity is forced towards the counter electrode by the electric fields and in our case air flow into the vacuum chamber. During the flight solvent evaporates, but the droplet charge remains constant. When the electrostatic repulsion force between the charges becomes equal to the force from the surface tension which is holden the droplet together, droplets split up into smaller droplets. This process is called Coulomb fission. At this point the "Rayleigh stability limit" is reached that can be expressed with the Rayleigh equation [12, 23]:

$$q_R = 8\pi(e_0\gamma R^3)^{1/2} \tag{2.3}$$

where q_R is the excess charge on the droplet of radius R, γ is the surface tension and e_0 is the permittivity of vacuum. Through the Coulomb fission process charge density and so the repulsion force between the charges decreases under the Rayleigh limit and the resulting droplets are stable again.

The Coulomb fission process repeats several times until only one single macromolecule is existent in each droplet. As the final step in the tran-

sition from droplets to a gas-phase ions two models exist: The charge residue model (CRM) suggest that electrospray droplets repeat several evaporation and disintegration cycles until only small droplets containing only one ionized macro-molecule exist. Through evaporation of the remaining solvent molecules a gas-phase ion remains. In the ion emission model (IEM) it is assumed that single ions are emitted from larger droplets. These ions reduce the charge density in the emitter droplet and reestablish stability in the emitting droplet. Results where Fernandez de la Mora found usually multiply charged ions [7] indicate the CRM for large molecules over 3300 Da (1Da = 1u $\approx$ Mass of a single Hydrogen atom). Wang and Cole [4, 34] found out that a higher solvent polarity leads to more multiply charged ions. And Kebarle et al. [13] found originally negative ions charged positively and vice versa. This indicates that the analyte molecules are charged by excess charges present in the final droplets, no matter of their initial charge.

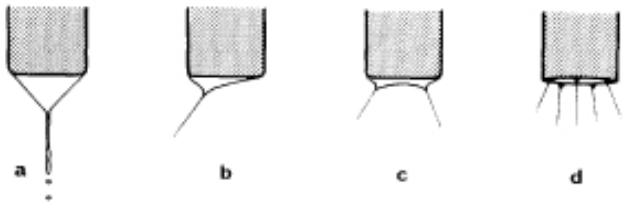

Figure 2.2: Cone-jet modes of electrospray ionization, obtained from [2]. With the right voltage applied a perfect Taylor-cone forms and a fine spray of droplets is produced (a). Increasing the voltage leads to a off-centered (b) cone and then to multi-jet modes (c, d).

M. Coupeau and B. Prunet-Foch [2] did an extensive series of experiments to determine the influence factors for electrospray ionization. They found out that a stable electrospray with the formation of a spray of droplets of nearly identical diameters depends on the conductivity of the solution, applied voltage, flow-rate, capillary geometry and capillary wettability. All these parameters can only be varied within a narrow range, otherwise the "perfect" Taylor cone (figure 2.2 (a)) is not possible and not useful multi-jet modes (figure 2.2c,d) or large uneven droplets are resulting.

To conclude this chapter, it is to say that electrospray ionization is compared to other ionization methods 'softer' [3]. Even complexes with weak non-covalent bindings that exist in solution can be studied in gas-phase [18, 19, 22]. All these above listed properties make electrospray ionization a very versatile technique to ionize all kinds of molecules, but specifically large complexes of organic molecules.

3 MOLECULEWRITER PROTOTYPE APPARATUS

3.1 Overview

The main goal of the described electrospray ionization (ESI) prototype apparatus is to deposit 3D patterns of large molecules like proteins on a surface. Being able of that, complex 3D structures in a nanometer range can be achieved opening the path for totally new future applications. The approach is to generate a beam of charged molecules (ion beam) that can be controlled by electrostatic forces similar to the electron beam in a TV. The target of the beam where the molecules are deposited has to be in a high vacuum to avoid impurities that will disturb the deposited structure's properties. The ion beam is created at atmospheric pressure, because electrospray does not work in vacuum, and passes several differential pumping stages (vacuum chambers) with decreasing pressures and filtering, focusing and deflection mechanisms until it reaches the target chamber where the substrate is located at a ultra high vacuum.

Figure 3.1 shows the original design of the ESI prototype apparatus. In the *injection chamber* the ion beam is generated by the electrospray

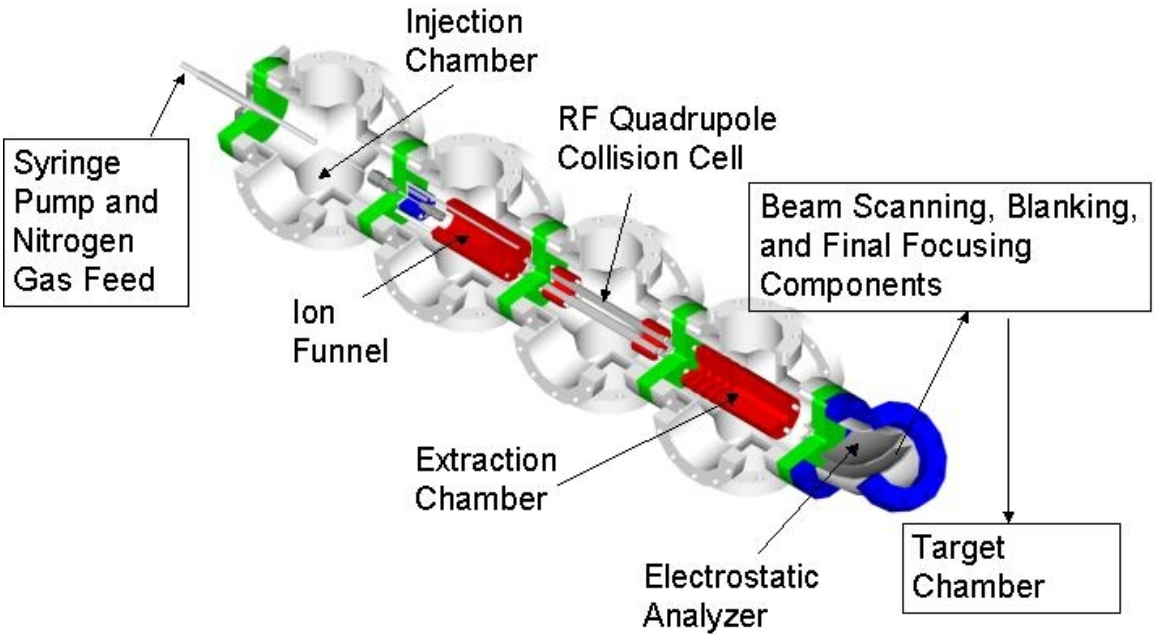

Figure 3.1: Original design of ESI patterning prototype system, obtained from Anthony Cascio.

process at atmospheric pressure as described in chapter 2. Nitrogen gas is used to accelerate the formation of ions from charged droplets. The ions are guided through a capillary into the first vacuum chamber including an *ion funnel*. With the rapid drop in pressure and due to repulsion of the ions of the same polarity from each other the ion beam spreads out. The ion funnel focuses the beam and prevents a loss of ions at the chamber walls.

After being focused in the funnel the ions enter the second vacuum stage. This stage is called *collision cell* and consists of a RF (radio frequency) quadrupole. Only ions with a certain mass-to-charge (m/z) ratio can pass through the quadrupole and all other ions collide with the

walls of the quadrupole and are so filtered out. The remaining ions with the desired mass-to-charge ratio pass the *ion extraction chamber* and an electrostatic analyzer chamber, where only ions with a desired speed can pass through. From there the ions get into the final stage where the components for *beam scanning* (deflection of the beam), *blanking* (shutting the beam "on" and "off") and *final focusing* are before they hit the *target substrate*.

3.2 Electrospray unit

The most important part of the electrospray unit is the electrospray needle. Dimensions of the used needle are an outer diameter of 0.47mm at the needle tip and 0.72mm at the straight part of the needle. The inner diameter increases from 0.13mm at the needle tip to 0.15mm. For exact aligning of the needle, it is mounted on a xyz-stage adjustable by micrometers. A Stanford Research Systems PS350 high voltage power supply that can supply a voltage from -5kV to 5kV but only currents up to 5mA is connected to the needle.

During the development process a solution of acetonitrile and deionized water containing Coomassie Brilliant Blue dye molecules was used. The dye molecules are relatively large with molecular mass of $\sim$833 Da and result in blue deposition patterns, that make it easy to detect loss. Electrical conductivity of the solution can be controlled by the amount of deionized water added and was during the experiments at about 40 μS for

optimum electrospray performance. Flow-rate of the solution was controlled using a precision syringe pump from Harvard Apparatus. During the experiments the flow-rate was typically 0.3 mL/min.

To detect a stable electrospray a video camera with a magnification of 10 was used. Additionally a green laser beam was directed to the area in front of the Taylor cone to verify that a fine spray and not large non-uniform droplets or multi-jets were produced.

3.3 Vacuum interface

Originally the interface between the electrospray unit and the first vacuum chamber was implemented using a capillary. The typical capillary used for the experiments was 20cm long with an inner diameter of 0.5mm. It was mounted on the vacuum chamber opening using a Swagelok tube fitting. This construction allows easy and fast exchange of the capillary for cleaning purposes. Inside the vacuum chamber the capillary is hold in place by the heater construction. A plexiglass chamber around the electrospray needle and the capillary prevents air turbulence and can be filled with heated nitrogen gas to accelerate solvent evaporation.

3.4 First vacuum chamber and inside funnel

In the first vacuum chamber, also called first differential pumping stage, a typical pressure of $\sim$1 Torr is present due to the limited power of the vacuum pump and constant airflow into the chamber. Main part of

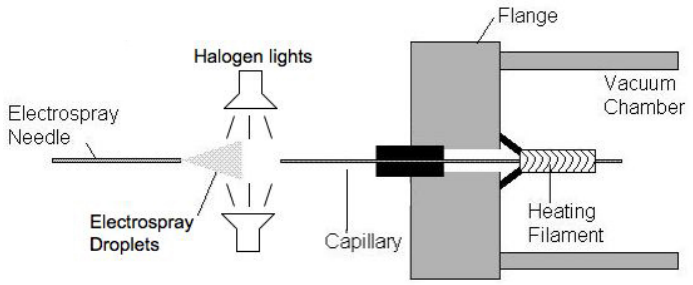

Figure 3.2: Vacuum interface: A capillary is mounted on the flange of the vacuum chamber using a Swagelok tube fitting.

the first vacuum chamber is the inside ion funnel. The ion beam entering this chamber through a capillary or orifice is widened up due to the rapid expansion in the chamber and Coulomb repulsion forces. To focus the diffuse ions back to a collimated ion beam the inside funnel has been designed building up on previous work of Julian et al. [11].

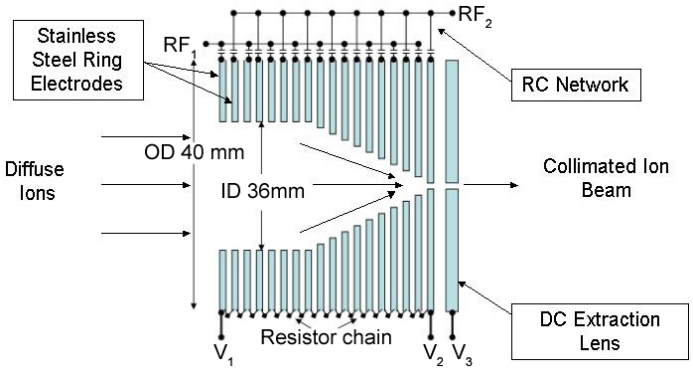

Figure 3.3: Schematic of the ion funnel. Ions enter the ion funnel from the left and get focused through the DC extraction lens on the right side.

A sine signal in the range of several kHz to MHz is applied to the even and odd lenses (RF1 and RF2). The signal on RF2 is 180 degree phase-shifted compared to RF1. This fact results in a strong electric field in the outer regions of the funnel driving the ions towards the middle

and a nearly field free region in the middle of the funnel. Due to the cone-shape the field free region gets smaller in diameter towards the end of the funnel focusing the diffuse ions into one spot at the funnel outlet. A static electric field is superimposed the RF field. Therefore a DC voltage is connected to V_1 and V_2. Through the resistors between the funnel lenses a field gradient pushing the ions towards the funnel outlet is generated. The capacities between RF voltage connector and lenses separate RF and DC voltage from each other. Last lens of the inside funnel is the DC extraction lens. A DC voltage applied to this lens can control the amount of passing ions and work as a shutter.

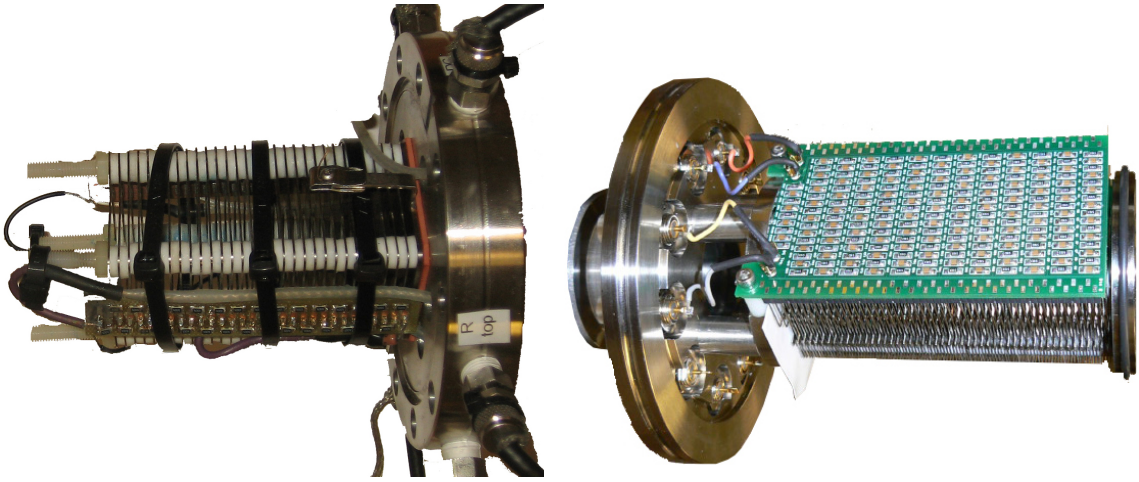

(a) Old ion funnel (b) Redesigned ion funnel

Figure 3.4: Old and redesigned ion funnel. The ions enter both funnels on the left end exit through the right side.

Concluding this section the main tasks of the inside funnel are generating a collimated ion beam out of the diffuse ions in the vacuum chamber and filtering out uncharged particles that are not useful for the further

process. Uncharged droplets or solvent molecules are not influenced by the electric field and so they hit the lenses of the ion funnel and are filtered out. Connecting the DC outlets to a picoampere meter allows to measure the ion current hitting the funnel.

3.5 Second vacuum chamber and Faraday cup

As the pressure could be reduced from atmospheric pressure (∼750 Torr) to 1 Torr in the first differential pumping stage, an additional turbo pump in the second vacuum chamber is able to reduce the pressure down to 15 mTorr. This pressure reduction is crucial for the deposition of ions in this prototype: The lower the pressure the longer is the mean free path of the ions and the longer is the distance the ions can flight without bumping into other molecules where they get deflected and their velocity decreases. If the mean free path is too short and there is no additional force accelerating the ions they stop and do not reach the deposition substrate.

In the actual development state the only part in this chamber is a Faraday cup: A metal cylinder closed at the end is connected to a picoampere meter to measure the ion current after the inside funnel. These measurements were used to calculate the efficiency of the inside funnel and to optimize the voltages of the inside funnel.

3.6 Current requirements for the electrospray deposition

In order to determine the necessary ion current to make depositions in a fairly short time, consider the following example:
Assuming the area of 1cm^2 shall be coated with 1 monolayer of cytochrome c, how long would it take to do the deposition with an ion current of 1, 2, 4 and 8nA? With the simplifying assumption that the irregular shaped protein cytochrome c is a sphere with a diameter of 3.1nm [20], the number of molecules per cm^2 can be calculated:

$$\frac{molecules}{cm^2} = \frac{1cm^2}{(3.1 \cdot 10^{-7}cm)^2} = 1.04 \cdot 10^{13} \tag{3.1}$$

The measured electrical current can be converted into molecular current (molecules per time) using the following formula:

$$\text{Molecular current } = \frac{\text{electrical current}}{\text{charge state} \cdot \text{elementary charge e}} \tag{3.2}$$

According to Iavarone et al. [10], who used a solution similar to the one used in the later experiments, the most intense charge state for cytochrome c sprayed in a 47:50:3 water:methanol:acetic acid solution in positive ion mode is 16^+ with a maximum of 19^+ and a minimum charge state of 11^+. Using equations 3.1 and 3.2 an electrical current of 1nA at a charge state of 16^+ correlates to $0.39 \cdot 10^9$ molecules/second (2nA: $0.78 \cdot 10^9$; 4nA: $1.56 \cdot 10^9$; 8nA: $3.13 \cdot 10^9$). These molecular currents equal

depositions times of 7.4h (1nA), 3.7h (2nA), 1.85h (4nA), 56min (8nA). So the goal is to get a high current of large molecules at a low charge state in order to make fast and economical depositions and patterns.

4 RESULTS AND DISCUSSION FIRST PROTOTYPE APPARATUS

4.1 Results from previous work

Previous work [28] disclosed very large improvement possibilities in the used electrospray setup. A loss of 99 % of the emitted electrospray current was credited four major sources:

- Ionization efficiency during the electrospray process - too large droplets
- Expanding plume between electrospray needle and vacuum
- High loss inside the vacuum interface capillary
- Low efficiency of the inside funnel

During this work it was tried to improve the low performance of the electrospray system with three measures: Heated gas streaming from capillary to electrospray needle and capillary heating were implemented to improve the droplet evaporation rate thus resulting in smaller droplets or ideally gas-phase ions inside the ion funnel chamber. The low efficiency of the inside ion funnel could be improved from 10 % to 45 % resulting in a Faraday cup current I_{FC} of 930 pA.

Since a high ion current into the Faraday cup results in a short deposition time it was tried as a next step to increase the current I_{Funnel} into the ion funnel. Replacing the 15 cm long capillary by a 1.5 mm thick cone-shaped orifice the current into the ion funnel I_{Funnel} could be increased from 2 nA to 100 nA which is 50 % of the total emitted electrospray current. Despite the high current intensity it was impossible to focus any of the ion funnel current I_{Funnel} into the Faraday cup, probably because a high space charge field inside the funnel and large droplets because of the missing heating.

The third measure was to implement an electrostatic ion funnel between electrospray ion source and inlet orifice. It was built similarly to a design of Saf et al. [24] to focus the expanding electrospray plume into the inlet capillary. The outside funnel should enable larger distances between electrospray source and orifice resulting in smaller droplets or gas-phase ions at the vacuum inlet orifice - large or frozen droplets were suspected to be the reason for the low ion funnel performance [28]. It was possible to maintain an ion current I_{Funnel} of 2.8 nA, but the maximum current into the Faraday cup I_{FC} was 300 pA or 10 %.

The results gained from this previous work indicate a high importance of a moderate heating inside a vacuum interface capillary that results in small droplets or even fully evaporated gas-phase solute ions inside the ion funnel chamber. Increasing the distance between electrospray

source and vacuum inlet using an electrostatic ion funnel emerged to be impractical and inefficient compared to a heated capillary in combination with a heated gas stream.

4.2 Characterizing the existing prototype setup: droplet evaporation problems

Building on the results of the previous work, an extensive set of experiments was done to characterize the electrospray deposition prototype apparatus. These experiments should focus specifically on the droplet evaporation problem which is suspected to be the main cause for the low performance of the vacuum interface capillary and the electrodynamic ion funnel inside the first vacuum chamber. Three main parameters were varied during the experiments:

- Pressure inside the vacuum chamber
- Distance between electrospray needle and capillary
- Temperature around the inlet capillary

4.2.1 Pressure variation

To determine the best pressure to operate the ion funnel three experiments were performed during which the pressure in the first vacuum chamber was varied using the gate-valve between chamber connection and vacuum pump. The temperature was varied using the two halogen lights. Brilliant blue dye was sprayed in a solution with 9:1 methanol:water, con-

ductivity 35 μS, using the standard metal needle against a 30 mil[1] inner diameter, 15 cm long stainless steel capillary at a flowrate of 1 μL/min. The results of these experiments are displayed in figure 4.1. The total

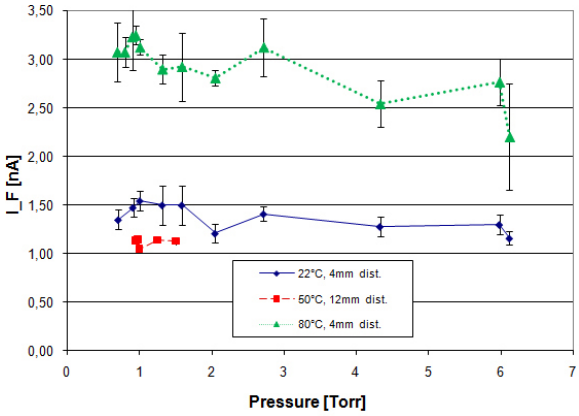

(a) Total current into ion funnel

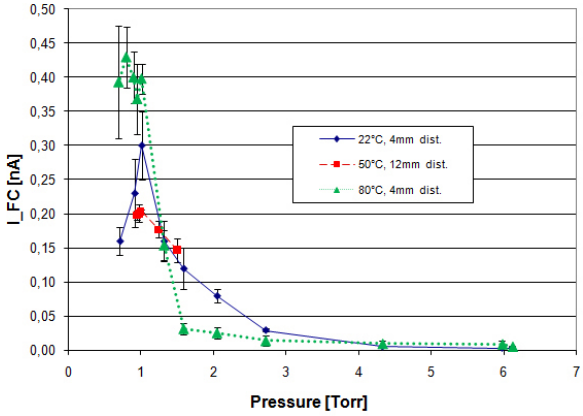

(b) Current focused into Faraday cup

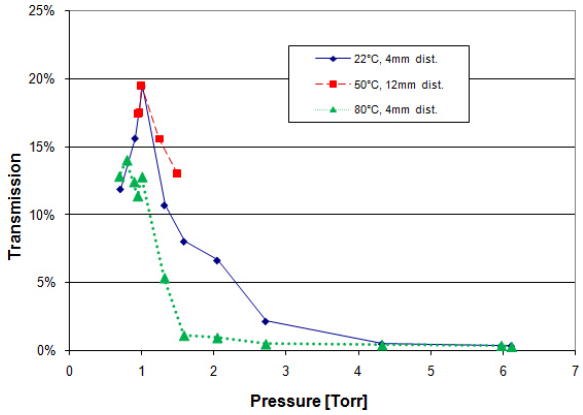

(c) Ion funnel transmission

Figure 4.1: Pressure dependencies at different temperatures. Whereas the total current into the vacuum chamber does not show a significant pressure dependency, the transmitted current through the ion funnel is very dependent on the pressure and shows a narrow peak around 1 Torr.

current into the ion funnel I_F remains nearly constant over the pressure range from 0.71 to 6 Torr. Heating to 80 °C at a distance of 4 mm be-

[1] 1 mil = 1/1000 inch = 0.0254 mm

tween electrospray needle and capillary increases the current by a factor of two compared to room temperature. Increasing the distance to 12 mm results in a lower total current into the chamber which can be explained by the expanding electrospray plume. The electrospray current simply spreads out over a larger area and more molecules get neutralized at the chamber walls around the inlet capillary.

Unlike the total current the transmitted current into the Faraday cup I_{FC} has a very strong pressure dependency. For all measured temperatures and distances there is a very narrow peak around the pressure of 1 Torr. This is consistent with results from previous work [28], but other research groups have different experiences. Julian et al. [11] could observe a working range of a similar ion funnel "from several torr to 50 millitor".

Since it is our goal to maximize the total current into the Faraday cup the best conditions are a pressure of 1 Torr and electrospray with a small distance (4 mm) between needle and inlet capillary at a temperature of 80 ℃. These conditions result in a maximum current of 430 pA in the Faraday cup.

4.2.2 Distance variation

After determining the best pressure to operate the ion funnel the best distance between electrospray needle and inlet capillary should be found. This distance is a very important factor for the transformation process from charged microdroplets to free gas-phase ions. At atmospheric pres-

sure the mean free path is 68 nm, resulting in ∼60000 collisions between the microdroplet and air molecules along the 4 mm distance between needle and capillary. At 1 Torr pressure inside the first chamber the distance has to be 760× as long as at ambient pressure to result in the same number of collisions. The number of collisions influences the evaporation speed of the microdroplet and so the ion formation time. With a 760× higher mean free path inside the first vacuum camber almost all evaporation has to occur outside the chamber and inside the capillary.

In preparation of a distance experiment the needle was moved to a position flush with the capillary opening with the help of the microscope camera (capillary inner diameter is larger than needle outer diameter). A ruler was adjusted to the zero position on the apparatus table to allow accurate distance measurements at the needle fixture. The total current into the vacuum chamber I_F and the current into the Faraday cup I_{FC} were measured at a temperature of 22 ℃, 50 ℃ and 80 ℃. Brilliant blue dye was sprayed in a solution with 9:1 methanol:water, conductivity 35 μS, using the standard metal needle against a 30 mil inner diameter and 15 cm long stainless steel capillary at a flowrate of 1 μL/min. The pressure in the ion funnel chamber was kept constant at 1 Torr.

Figure 4.2 presents the results of the distance experiments. The total current into the ion funnel over distance is almost the same for a temperature of 50 ℃ and 80 ℃ with a maximum current of 3.75 nA and 3.89

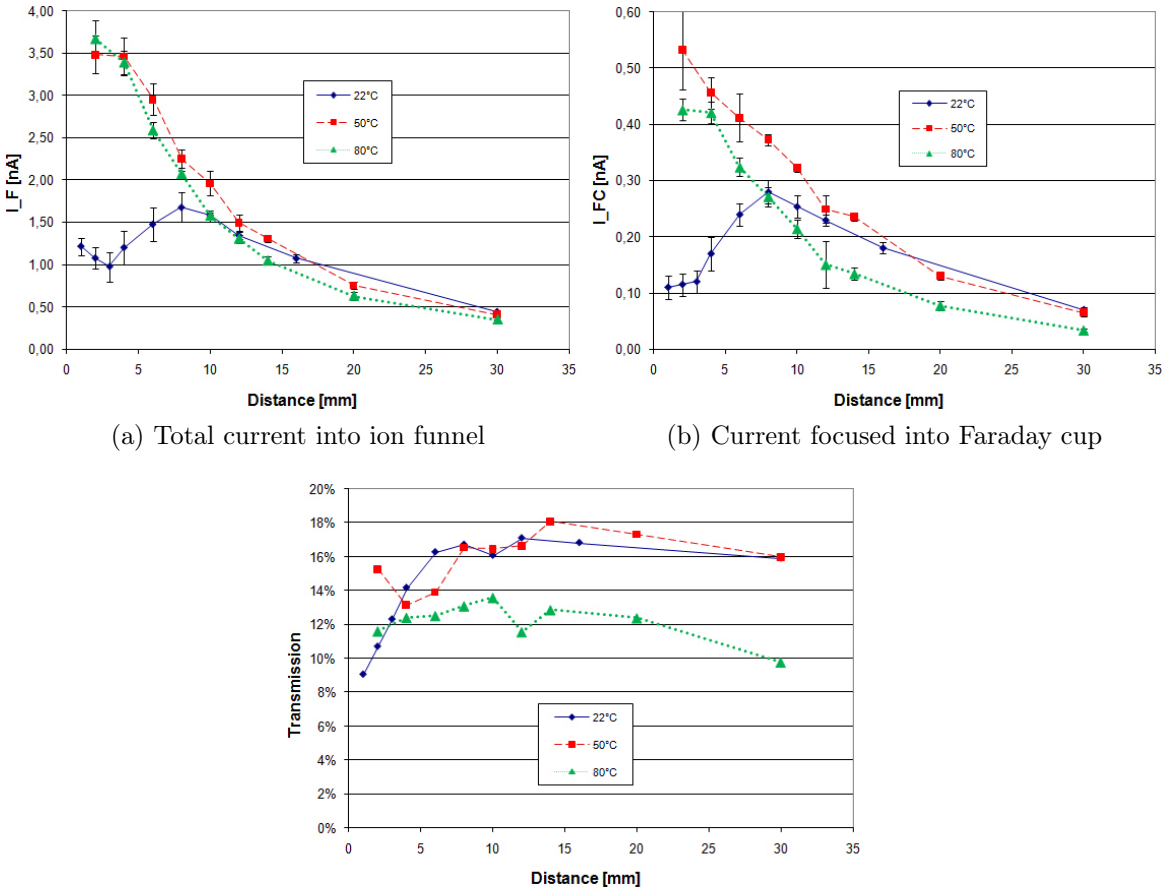

(a) Total current into ion funnel

(b) Current focused into Faraday cup

(c) Ion funnel transmission

Figure 4.2: Distance dependencies at different temperatures. At a distance larger than 8-10 mm between electrospray needle and capillary heating shows no additional influence on droplet evaporation.

nA at 2 mm distance. It drops almost exponentially with increasing distance. At room temperature the current decreases between 1 and 3 mm, then increases until 8 mm. From there the current at room temperature is equal to the currents with heating involved.

The ion currents into the Faraday cup follows almost exactly the same shapes of the total currents. At 50 ℃ and 80 ℃ there is again an exponential decrease with increasing distance an at 20 ℃ the current increases

between 1 and 8 mm distance and is similar to the two other curves between 10 and 30 mm. The transmission through the ion funnel remains fairly constant with varying distance, except for the current at room temperature, where the transmission increases linearly between 1 and 6 mm and then remains constant.

These experiments demonstrate that the distance between electrospray needle and vacuum inlet capillary as well as the temperature play an important role in the droplet evaporation process. Specifically for short distances heat can improve droplet evaporation remarkably. At a distance around 8-10 mm collisions with air molecules have contributed so much to the evaporation process that heating has no additional effect. But because of the expanding electrospray plume a short distance is desired, where a larger percentage of the molecules gets transferred into the vacuum chamber, though heating is needed to support solvent evaporation from the droplets.

4.2.3 Temperature variation - Effects of positive and negative ion mode and the difference between 20 mil and 30 mil capillary

After determining the importance of heating and a close distance between electrospray needle and capillary from previous experiments, three major experiments were done to determine the influence of heating in combination with negative and positive ion mode and 20 and 30 mil inner

diameter vacuum inlet capillaries. In all experiments the standard brilliant blue dye solution (solvent 9:1 methanol:water, conductivity 35 μS) was sprayed with the standard metal needle at a flow rate of 1 μL/min. The distance between needle and capillary was held constant at 4 mm and all capillaries had a length of 15 cm. The pressure inside the ion funnel chamber was constant at 1 Torr.

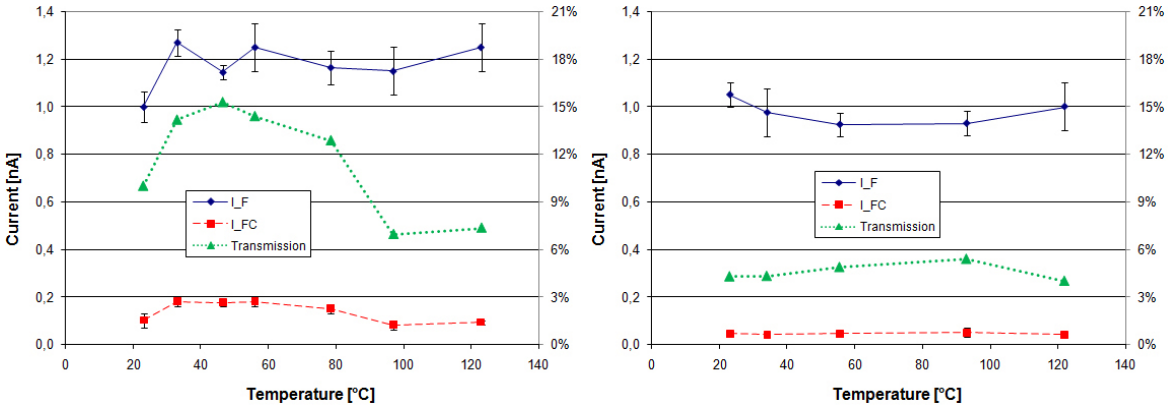

(a) Negative ion mode

(b) Positive ion mode

Figure 4.3: Negative vs positive ion mode with a 20 mil capillary. In negative ion mode the best transmission is observed between 33-56 °C. The very low and not temperature dependent Faraday cup current in positive ion mode indicates that only negative charge states exists for brilliant blue dye in 9:1 methanol:water solution.

Figure 4.3 shows the comparison of a 20 mil versus a 30 mil inner diameter capillary. The total current (absolute values) is almost constant at 1.2 nA for negative ion mode and 1.0 nA for positive ion mode. In positive spray mode the current into the Faraday cup I_{FC} showed no temperature dependency and was constant at the very low value of 40-50 pA, resulting in a transmission of about 5 %.

In negative ion mode however I_{FC} showed a strong temperature dependency. A temperature of 33-56 ℃ increased the Faraday cup current from 100 pA at room temperature to 180 pA and the funnel transmission from 10 to 15 % . Higher temperatures than 80 ℃ let the transmitted current I_{FC} decrease to 80-90 pA, a transmission of 7 % .

This result indicates that the brilliant blue dye molecules are not positively charged in our solution and the current in positive ion mode only consists of solvent molecules which have a mass-to-charge ratio that cannot be focused by the ion funnel. In negative ion mode the negatively charged dye molecules contribute to the electrospray current and so a higher transmission through the ion funnel is achieved.

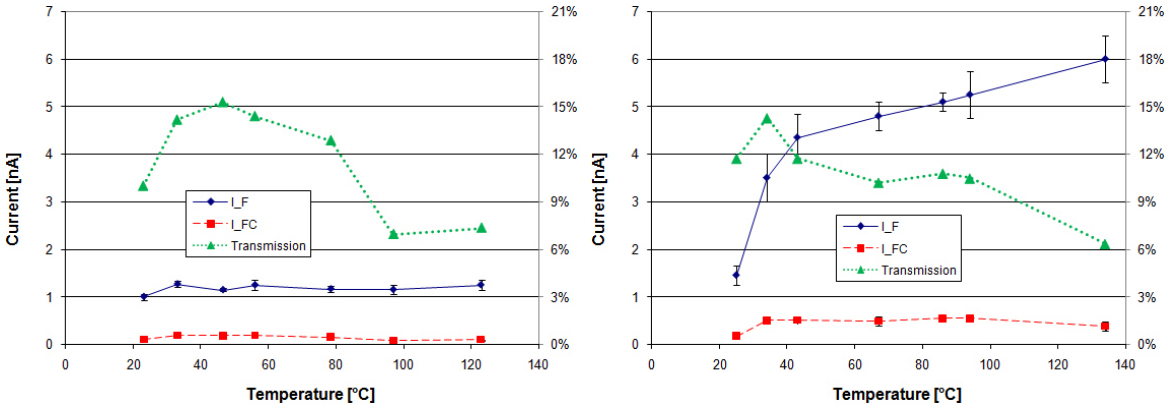

(a) 20mil (b) 30mil

Figure 4.4: Comparison of a 20 mil and 30 mil capillary in negative ion mode.

In the third experiment the brilliant blue dye solution was sprayed against a 30mil capillary in negative ion mode. The differences between 20 and 30 mil capillary in negative ion mode are displayed in figure 4.4.

The total current into the ion funnel I_F increases rapidly between 22 and 43 ℃. Over 43 ℃ I_F follows a linear increase with temperature resulting in a maximum current of 6 nA at 134 ℃. The transmitted current I_{FC} follows a similar incline between 22 and 33 ℃ from 170 to 500 pA and remains nearly constant between 43 and 94 ℃.

This experiment shows that a larger capillary diameter leads to a higher and more temperature dependent total and transmitted current. But other groups, e.g. Kim et al. [14], observed transmitted currents over 3 nA after the ion funnel.

4.3 Discussion

The results of this series of experiments have revealed a strong pressure dependency of the used ion funnel. Whereas other experiences [1, 11] showed that similar ion funnels were able to operate at a wider pressure range. This problem could be related to unfavorable gas stream inside the vacuum chamber and problems in the droplet evaporation process. Recondensation of droplets [35] or frozen droplets due to the rapid gas expansion inside the vacuum chamber were suspected to counteract the ion formation and decrease the ion funnel efficiency.

This theory is supported by the results of the distance variation and heating experiments. Increasing the distance between electrospray needle and inlet capillary and moderate heating result in higher transmission

through the ion funnel. Shaffer et al. [26] could observe that solvent related current and large droplets are effectively filtered out by the ion funnel. Heating the inlet capillary only from the outside with halogen lamps also creates a large temperature gradient over the capillary that could increase recondensation and loss inside the capillary.

The low overall performance of the prototype configuration compared to other system lead to a redesign of the prototype which is described in the following chapter.

5 REDESIGN OF THE PROTOTYPE APPARATUS

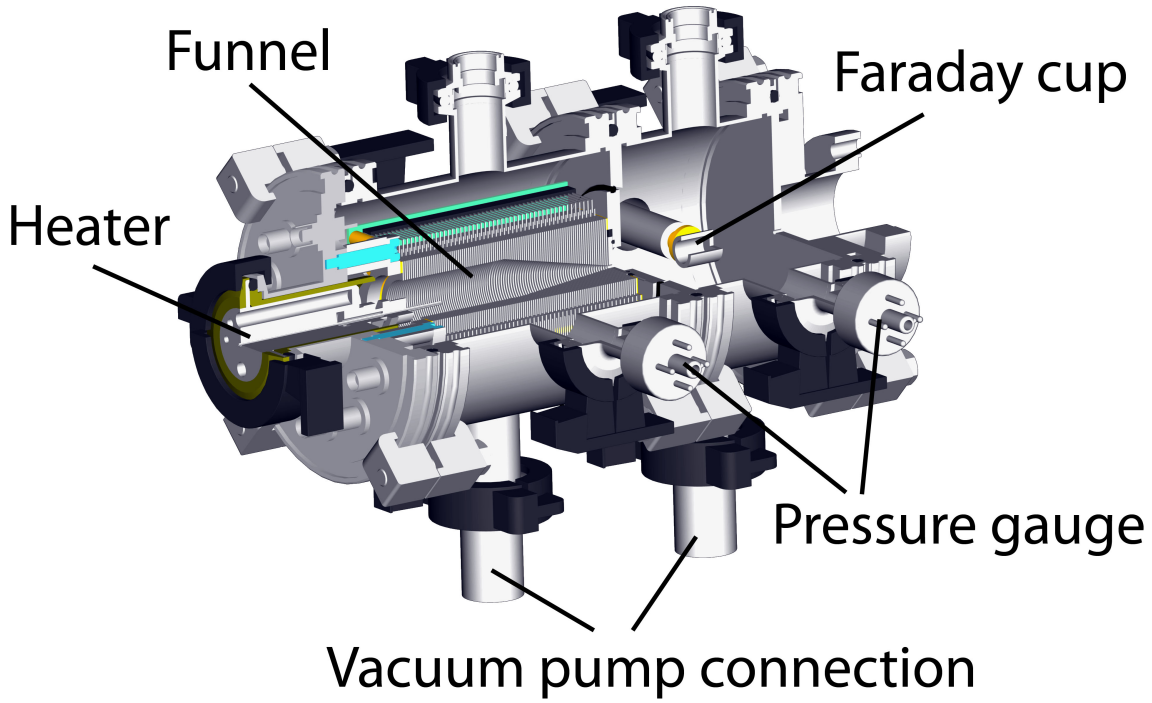

Figure 5.1: New prototype system, obtained from Florian Kaiser: A more compact and easier to reassemble design was chosen. The vacuum interface is a capillary hold by a solid aluminum heater block. In the first vacuum chamber contains the ion funnel at a pressure of 3-6 Torr. The second vacuum chamber contains the Faraday cup to measure transmitted current through the funnel. This chamber will be replaced with a quadrupole ion guide in the next design cycle.

Due to the low performance of the old prototype setup and specifically the capillary heating and the ion funnel a major redesign was considered. The main requirements were a more uniform heating of the capillary and

a stronger ion funnel to handle higher space charge with less influenced of the gas flow inside the chamber. Figure 5.1 shows the new prototype apparatus design. The ion funnel chamber was custom made, adjusted to the length of the new ion funnel. (SPECS Technologies Corporation, Sarasota, FL). NW 100 ISO flanges are used as the large diameter interconnects and KF 25 Kwik flanges are used for all connections perpendicular to the chamber axis. To fit the heater block the front flange is equipped with a KF 40 flange. Hermetic sealed BNC connecters were used in the front flange for electrical connection of two DC voltages and two RF signals to the PC board.

The new ion funnel was designed similarly to the funnel that Belov et al. [1] presented. The main difference to the old ion funnel is the smaller distance between the funnel lenses and the higher manufacturing precision. The smaller distance between the lenses results in a higher field strength near the inside edge of the funnel. As a result the restoring force on ions in the outer regions of the funnel is larger compared to the old ion funnel. This results in a larger pressure range and a higher transmission specifically for space charge dominated ion beams. Figure 5.2 shows the funnel drawing.

The new ion funnel consists of 100 lens electrodes made of 0.5 mm thick stainless steel. The lenses are aligned and hold by four ceramic rods and separated by 0.5 mm thick teflon washers. The lenses are enclosed by a

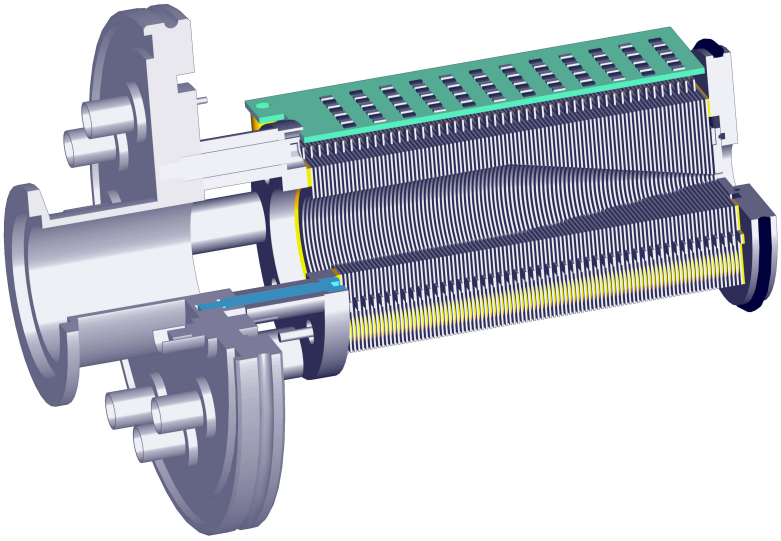

Figure 5.2: Cross-section of the new ion funnel, obtained from Florian Kaiser. The strait part consists of 55 lenses with a 25 mm diameter hole in the center. Over the next 45 lenses the hole diameter decreases linear from 25 mm to 2 mm. Each lens has a thickness of 0.5 mm and the lenses are separated by 0.5 mm thick teflon washers. The lenses are aligned by 4 ceramic rods. and enclosed by a stainless steel front- and endplate. Electrical connection to the lenses is made through BNC feedthroughs in the front flange and a circuit board that connects via steel wires spot-welded to the lenses.

stainless steel front- and endplate. The frontplate is bolted to the front flange of the vacuum chamber and the endplate with a surrounding o-ring seals the first vacuum chamber against the second one.

RF and DC signals are applied to the lens plates using a circuit board. This board contains the same RC network described in figure 3.3. All funnel lenses are connected in series with 0.5 MΩ resistors. These resistors create a linearly decreasing electrical potential in the funnel according to the voltage divider rule. This potential drop drives the ions towards the end of the funnel. Changing the voltage difference between funnel top

and bottom the ion velocity can be adjusted (higher potential difference means higher velocity).

Special focus was on a new heater design that should result in a more uniform temperature distribution across the stainless steel capillary. It also should be optimized for shorter capillary length as the capillary is suspected to be responsible for the largest part of lost ions.

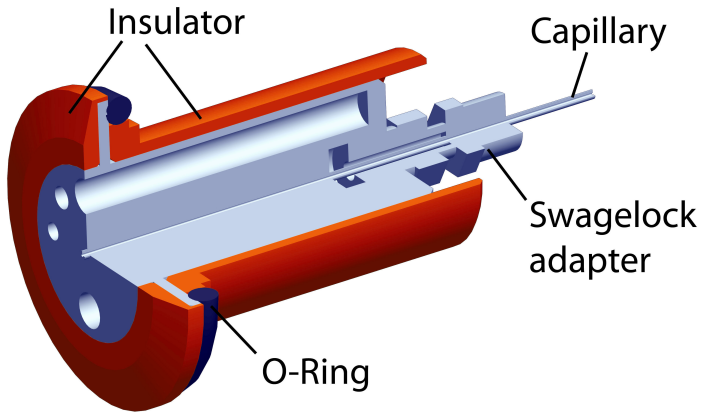

Figure 5.3: New heater design, obtained from Florian Kaiser.

The current heater design is shown in figure 5.3. It consists of a custom made aluminum block with two holes for cartridge heaters (upper cavity in cross section), one for a thermocouple to control the temperature in the block and the center hole for the capillary. The vacuum inlet capillary (Upchurch Scientific, Oak Harbor, WA) is hold in place and sealed by a swagelock fitting (Florida Fluid System Technologies, Sunrise, Fl) that is placed at the vacuum end of the block to allow shorter capillaries. The end of the fitting is flush with the funnel entrance. Thermal and electrical insulation from the vacuum chamber metal is implemented by a custom

made teflon surrounding. For ease of use the heater is sealed with a viton o-ring and is hold in place by the pressure difference between atmospheric pressure and vacuum chamber pressure (no difference could be observed using a Kwik flange KF clamp, MDC Vacuum Products, Hayward, CA). To exchange or clean the capillary only the vacuum pumps have to be turned off and the heater block can be slid out.

Temperature control of the heater block is implemented by using a Eurotherm 2132 PID-controller. A thermocouple that can be slid into the heater block provides temperature reading and two 175 Watt cartridge heaters (OMEGA Engineering, INC., Stamford, CT) enable fast heating over 200 ℃. Heaters and PID controller are 110 V powered and the heating power is controlled using a solid state relay connected to the puls-width-modulation port of the controller. The heater works excellent and is able to reach a temperature of 200 ℃ within about 2 minutes and can hold it within 5 ℃.

6 RESULTS AND DISCUSSION REDESIGNED PROTOTYPE APPARATUS

6.1 Commencement of the redesigned prototype

After physically building the new prototype a series of electrical measurements was made to ensure proper functionality of the RC-network on the manufactured circuit board, functionality of the newly designed heater and proper feedthrough connections. All 100 capacitor values were measured and capacitors out of 10 % tolerance were replaced. To exclude design and manufacturing errors in the printed circuit board the fully assembled and mounted funnel was measured using an analog oscilloscope.

The results of this measurement and a schematic are shown in figure 6.1. Initial measurements did not show the expected linear potential decrease. Since all 100 resistors are connected in series the voltage drops 1/100 of the input voltage over each resistor according to the voltage divider rule. So the voltage U_{real} at the xth lens can be calculated to:

$$U_{real} = \frac{(100 - x)}{100} U_{input} \tag{6.1}$$

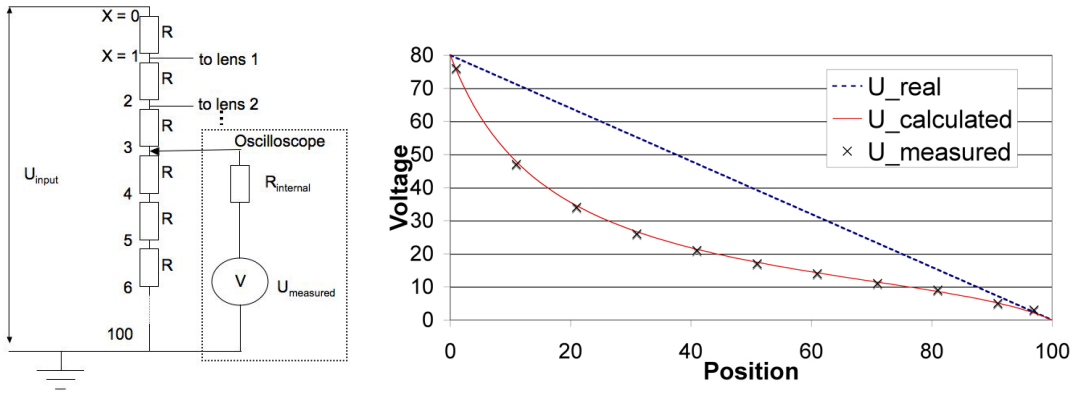

(a) Schematic of the funnel resistors

(b) Measured, calculated and real funnel lens DC voltages

Figure 6.1: Measurement error funnel resistors: The parallel resistance of the analog oscilloscope is in the magnitude of the funnel resistors and induces a large measurement error. Calculation the voltages after each resistor with the inner resistance of the oscilloscope in parallel results in correct values that can be verified by the measurement.

All resistors have a nominal value R of 0.5 MΩ. For the measurement a analog oscilloscope with a internal resistance $R_{internal}$ of 1 MΩ with a 10x probe is connected to the x_{th} funnel lens in parallel to the resistors. Because of the 10x probe the internal resistance is 10 MΩ which is in the magnitude of the total funnel resistance of 50 MΩ and so significantly distorts the measurement. The distorted voltage $U_{calculated}$ can be calculated and compared to the measured voltage $U_{measured}$:

$$U_{measured} = \frac{xR}{xR + R_{parallel}} U_{input}, \quad R_{parallel} = \frac{(100 - x)R \cdot R_{internal}}{(100 - x)R + R_{internal}} \tag{6.2}$$

Measurement and calculation are consistent hence the voltage drops over the resistors is linear and the correct function of the circuit board is proven.

As a first test a solution of brilliant blue dye in methanol with a conductivity of 80 μS/cm was sprayed with the standard metal needle through a 20 mil inner diameter, 15 cm long capillary in negative ion mode at a distance of 3 mm. The temperature was increased from 20 ℃ to 200 ℃ (Figure 6.2 (a)). With increased temperature less volume flows into the vacuum chamber because of gas expansion. While the pressure inside chamber 1 dropped linear from 1.71 Torr (22 ℃) to 1.44 Torr (200 ℃) the current also decreased from 2 nA to 1.5 nA. This indicates that the gas flow through the capillary is the dominant factor in the ion/droplet transport into the vacuum chamber. But limited by pumping power and the maximum operation pressure of the ion funnel a 30 mil diameter turned out to be a good compromise for a good current into the vacuum chamber.

To take advantage of the new heater design a 11 cm long 20 mil diameter capillary was used for the second experiment shown in figure 6.2 (b). The total current into the ion funnel was 3.0 nA at 24 ℃ and 3.1 nA at 200 ℃. Over the first 28 minutes the current into the Faraday cup increased almost linear over time with no funnel voltage connected (funnel floating). Then the temperature was slowly increased to 200 ℃ at 53 minutes. The Faraday cup current decreased with higher temperature and remained constant again after the temperature was kept constant at 200 ℃ (0:56 - 1:06).

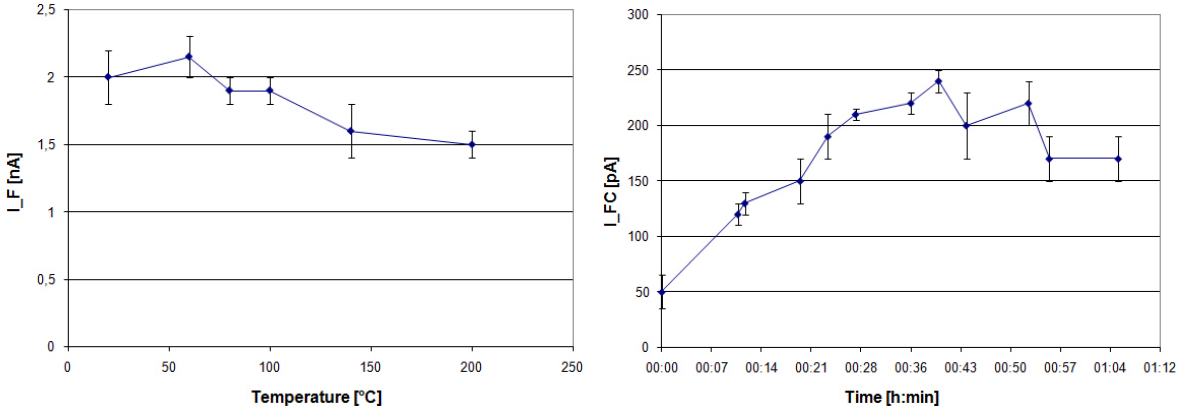

(a) Total funnel current with blue dye:methanol solution

(b) Current into the Faraday cup over time. Funnel current was 3 nA.

Figure 6.2: First test runs with new prototype: Brilliant blue dye molecules solute in methanol were sprayed. Current in (a) decreases with increasing temperature. In (b) the current into the Faraday cup was measured with the funnel not connected. A self-charging effect can be observed, but the current decreased after heating was started at 28 minutes.

The increasing current into the Faraday cup indicates a slight self charging effect of the ion funnel. Charged droplets hit the funnel lenses and reside there for a certain time. An equilibrium is reached when the static electric field from the residing charges is strong enough to deflect the ions/droplets inside the funnel. Other research groups (e.g. Kremer et al. [15]) tried to use this effect to create a passive ion funnel for the use at atmospheric pressure.

In a series of short experiments the best parameters for the funnel parameters DC voltage on inlet lens, DC voltage on smallest lens, amplitude of the sine RF signal and frequency of the RF signal should be optimized for highest current into the Faraday cup. The solution was changed from blue dye in methanol to a 0.5 mg/ml solution of the amino

acid Gly-Gln in a 50:50:1 methanol:water:acetic acid to be able to achieve results comparable to literature values like Kim et al. [14]. It is problematic to spray solutions with a high water percentage with the used metal needle because of the high surface tension of water. For that reason a switch to nano-electrospray was necessary. Nano-electrospray refers to a process where the solution is sprayed at a flow-rate between 200 and 500 nL/min through a needle with a tip diameter of typically 5-100 μm [25]. Because of the higher ionization efficiency of nano-electrospray lower voltages (1000 - 2000 V instead of 3000 - 5000 V) can be used.

These experiments demonstrated currents between 7 and 10 nA into the funnel with a 10 cm long, 20 mil diameter capillary, but the ion funnel was not able to focus any of this current into the Faraday cup. But with a 30 mil diameter, 15 cm long capillary up to 500 pA of a funnel current of 1.4 nA could be focused at a temperature of 140 ℃. As these results are not nearly consistent with literature values it was tried to modify the airflow inside the ion funnel chamber to reduce turbulence and gas-flow perpendicular to the funnel axis as this was suspected to deflect the ions towards the vacuum pump.

6.2 Improving ion funnel transmission through modified air flow

6.2.1 Gas-flow simulations

Gas-flow inside the ion funnel chamber was suspected to effect the transmission efficiency negatively. To examine these effects the ion funnel including circuit boards was wrapped into plastic foil. The plastic wrap was placed under the sealing o-ring at the exit end of the funnel so that the gas inside the funnel could only exit back to the funnel inlet or through the funnel exit into the second vacuum chamber. To compare the effect of the wrapping a simulation with a simplified model of the funnel was made using the software COMSOL Multiphysics. For simplification atmospheric pressure was assumed at the capillary exit and the outflow at the pump was set to 250 L/min. The gas was modeled as an incompressible fluid with only laminar flow. Those simplifications certainly effect the accuracy of the results, but were necessary because of the complexity of the simulation.

Figure 6.3 shows the comparison between unwrapped and wrapped ion funnel. Inside the unwrapped ion funnel all molecules are exposed to vertical velocities of 30 m/s in the center and up to 80 m/s in the outer regions whereas all ions that get inside the wrapped ion funnel are only exposed to the electrical field. In both versions the rapid expansion

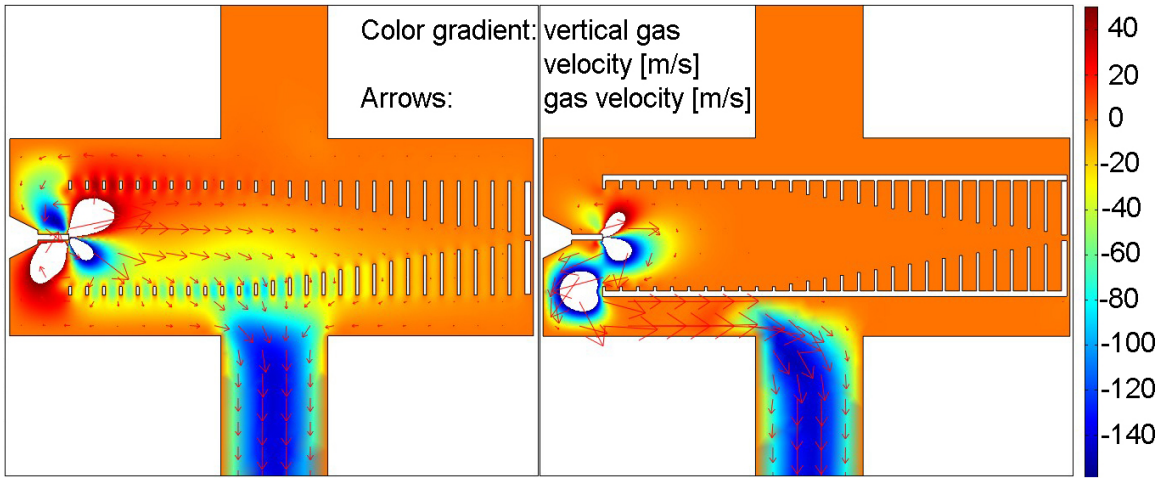

Figure 6.3: Simulated air flow inside the vacuum chamber: High vertical velocity (left) moves ions to the pump exit. This effect is not present in the wrapped funnel (right.) The white areas inside the funnel represent velocities outside the scale on the right.

after the capillary can be observed (white blobs in 45 degree angle at the capillary end). This rapid expansion and space charge are the main factors in widening up the ion beam and make the use of a focussing element inside the vacuum chamber necessary.

6.2.2 First experiment with the wrapped ion funnel

As a first experiment with the wrapped version of the ion funnel 0.5 mg/ml Gly-Gln in a 50:50:1 methanol:water:acetic acid (conductivity 140 μS) was sprayed with a flow rate of 300 nL/min. A 30 mil diameter, 10 cm long capillary was slowly heated from room temperature to 200 ℃. The end of the capillary was flush with the first lens of the funnel. A

sine RF signal with an amplitude of 100 V (200V peak to peak) and a frequency of 230 kHz was applied to the funnel lenses and the DC voltage gradient inside the funnel was 10 V/cm.

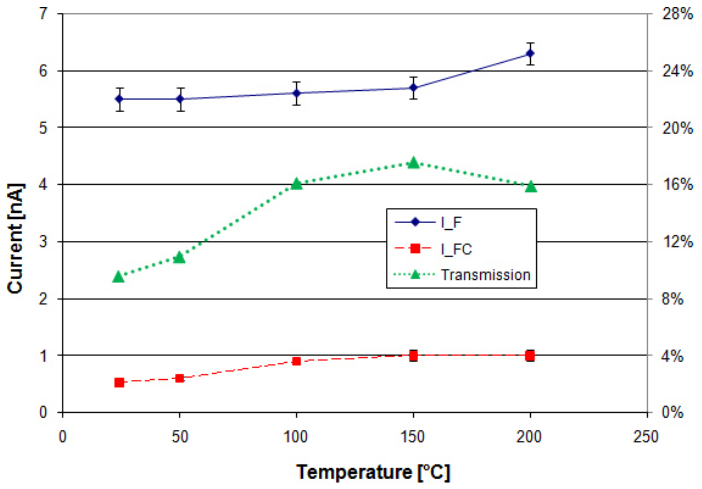

Figure 6.4: Funnel wrapped in plastic foil. Due to improved air flow a current of 1 nA can be measured at the Faraday cup (was 500 pA before).

The short 30 mil capillary results in a relatively high ion current into the funnel of 5.5 - 6.3 nA and the funnel is able to focus up to 1 nA into the Faraday cup. A maximum in transmission occurs at a temperature of 150 ℃ where it reaches 17.5 %. This result is encouraging to proceed with the wrapped funnel, but it is still far from literature values, where transmissions between 60 and 80 % are accomplished. It still has to be determined if there is a problem with the parameters like funnel frequency, amplitude, DC gradient, temperature and capillary length or if there is a problem with the design of the funnel itself.

6.2.3 Effect of the DC voltage gradient inside the funnel

Further optimization was tried by changing the voltage gradient that drives the ions towards the funnel exit. At a temperature of 200 °C the peak to peak voltage $U_{RF\ pk-pk}$ was increased from 0 V (no RF signal) to 250 V (maximum rating of the used capacitors) and the current into the Faraday cup was measured. Figure 6.5 (a) shows the current into

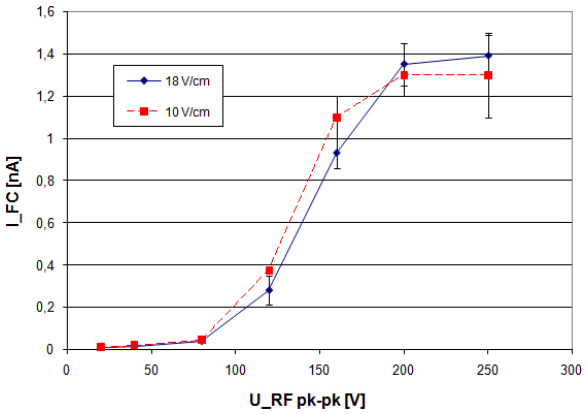

(a) Funnel wrapped into plastic foil

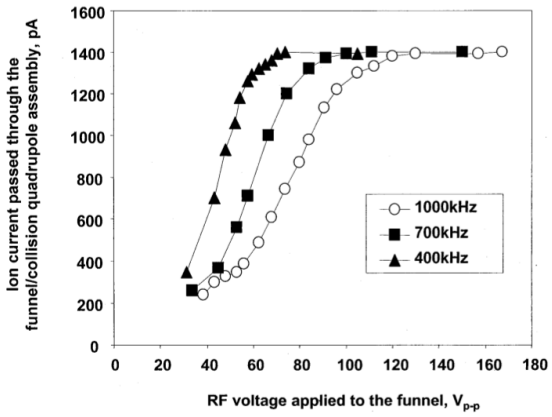

(b) Belov et al. [1]

Figure 6.5: Funnel wrapped in plastic foil to improve air flow: The results are comparable to other research groups.

the Faraday cup with a DC gradient of 10 and 18 V/cm. Out of a total current of 5.3 nA into the funnel 1.3 nA (10 V/cm) and 1.4 nA (18 V/cm) could be transmitted. Both currents are very close and saturate into a maximum above 200 V peak-to-peak voltage. The shape of the recorded curve is similar to comparable setups (b) with the difference that the amplitude needed to reach the maximum transmission is higher in our setup. But these result indicate a proper design of the ion funnel and

encourage to further optimization to reach higher transmissions up to 80 % and currents of up to 7 nA into the Faraday cup.

6.2.4 Effect of the capillary position

Thereafter the importance of the position of the capillary was studied. A 30 mil diameter, 10 cm long capillary was mounted first flush with the first funnel lens then sticking 10 mm into the ion funnel. It was suspected that ions get reflected at the funnel entrance since the potential there is higher than the capillary potential if the sine wave on the lens reaches a maximum. The results are displayed in figure 6.6.

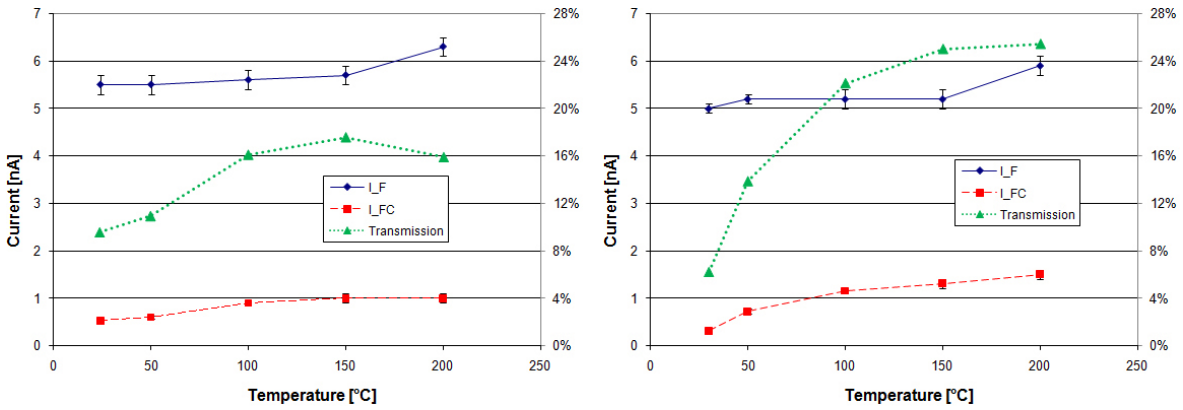

(a) Flush capillary (b) Capillary sticking 10 mm into funnel

Figure 6.6: Comparison of a capillary flush with the ion funnel entrance (a) and sticking 10 mm into the funnel (b). Better transmission is achieved if the capillary sticks into the funnel because there is no "potential hill" to overcome.

The currents into the ion funnel are very similar in shape and the little offset can be explained by a slight variation in the electrospray parameters, specifically the distance needle - capillary. But whereas the transmitted current reaches its saturation at 1 nA with the flush capillary,

it continuously increases with temperature and reaches a maximum of 1.5 nA at 200 ℃. Higher temperatures can not be used because of limitations of rubber and plastic elements. The transmission is about 1.5 times higher with the capillary sticking into the funnel compared to a flush capillary alignment with the first funnel lens.

This effect can be explained by the field energy that the ion entering the funnel has to overcome. The ion has a certain kinetic energy after it leaves the capillary. To get into the ion funnel the kinetic energy has to be larger then the field energy created by the potential difference between capillary and funnel. So in the best case the sine signal applied to the first funnel lens is at the minimum value (about -100 V with 200 V peak-to-peak RF signal). Then the potential of the first funnel lens (sum of RF signal + DC voltage applied to funnel entrance) is low and there is a force moving the ion towards the funnel entrance. But if the sine signal at the first funnel lens is at the maximum value (typically +100 V) there is a repelling force on the ion. This explanation is a simplification of the very complex interaction between gas flow, DC field and RF field between capillary and ion funnel, that requires extensive computer simulation for full understanding.

6.2.5 Summary of the first experiments

Resulting from this first series of experiments with the redesigned ion funnel first conclusions can be drawn. Modifying the air flow inside the

ion funnel by creating a gas-tight enclosure reduces disturbing gas flow perpendicular to the funnel axis and increases ion transmission. The DC gradient inside the funnel does not seem to play an important role, but the measured transmitted current over peak-to-peak RF voltage is comparable to literature, even if higher absolute voltages are needed for this funnel design. While the RF signal applied to the funnel lenses is intended to focus the diffuse ions entering the funnel towards the funnel center it can also repel ions before reaching the funnel. This effect does not show up in measurements of the total current into the ion funnel because there all DC and RF voltages are disconnected. Unfortunately the total current into the funnel can not be monitored with the existing equipment while running due to the measurement equipment and setup.

These results indicate a proper design of the ion funnel but the transmission values are too low compared to literature.

6.3 Excluding measurement errors at the Faraday cup

Resulting from the previous experiments a problem with the absolute transmission values emerges whereas the course of measured transmission curves is similar to literature. This indicates either a design error or a measurement error, e.g. not the total current is measured in the Faraday cup or the signal gets lost between Faraday cup and picoampere-meter. Until now the Faraday cup is centered in the second vacuum chamber about 8 cm away from the ion funnel exit. So there is a possibility that

a major part of the space-charge dominated ion beam misses the area of approximately 1 cm^2 of the Faraday cup. To investigate this behavior further the Faraday cup was extended so that the ion beam could be measured in a distance of about 5 mm behind the ion funnel exit. If not otherwise noted a 8.5 cm long, 30 mil inner diameter capillary was used. It was extending 1 mm into the ion funnel and sticking out 1 mm at the atmospheric side of the heater block. A nano-electrospary needle with an inner tip diameter of 30 μm was to spray the solution at a flowrate of 300 nL/min in a distance of 3-4 mm of the capillary.

6.3.1 Effect of the capillary length

The first experiment after extending the Faraday cup to the funnel exit orifice was measuring the transmitted current with different capillary lengths. Both capillaries had a inner diameter of 30 mil. The 10 cm long capillary was sticking 10 mm into the ion funnel whereas the 8.5 cm long one was aligned flush. A temperature of 150 ℃ was used to optimize droplet evaporation.

The result is shown in figure 6.7. Both capillary lengths result in an almost constant transmission from 150 to 800 kHz similar to the results of other research groups. A total current of 5.75 nA into the ion funnel was measured using the 10 cm capillary resulting in a maximum transmission of 46 % . The shorter 8.5 cm capillary results in less loss and leads also to a maximum transmission of 45 % of the higher total current of 6.6 nA.

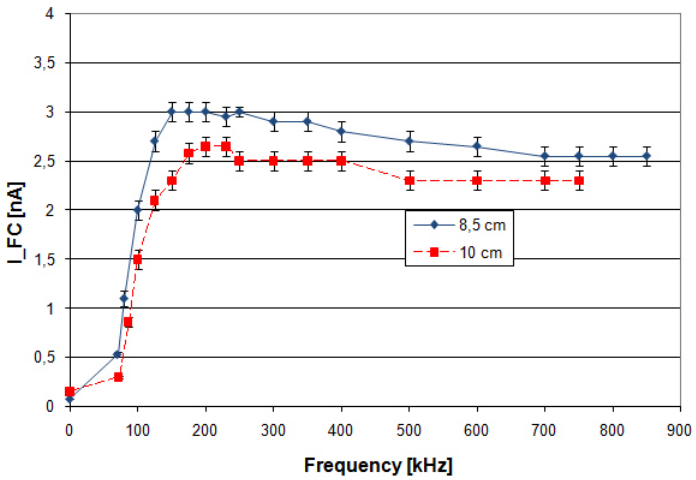

Figure 6.7: Comparison of current into the Faraday cup for 8.5 cm and 10 cm capillary. Total transmitted current is better for shorter capillaries.

6.3.2 Effect of the capillary diameter

Previous experiments with 20 mil diameter capillaries were not successful concerning transmitted current. Another experiment using the shortest possible length of 8.5 cm was set up since results from the capillary length experiment show better transmission for this length. 20 and 30 mil capillaries were compared at different capillary temperatures.

Whereas the total current into the funnel using the 8.5 cm capillary decreased from 7 nA at 24 ℃ to 2.7 nA at 150 ℃ and 2.4 nA at 200 ℃ increased the total current using a 30 mil capillary from 5.6 nA to 6.6 nA and 7.2 nA at 200 ℃ . The highest transmitted current was measured 0.8 nA (32 %) at 200 ℃ with the 20 mil diameter and 3.5 nA (47 %) with a capillary diameter of 30 mil. This experiment indicates that there is a problem using a 20 mil capillary in the used setup. Collisions

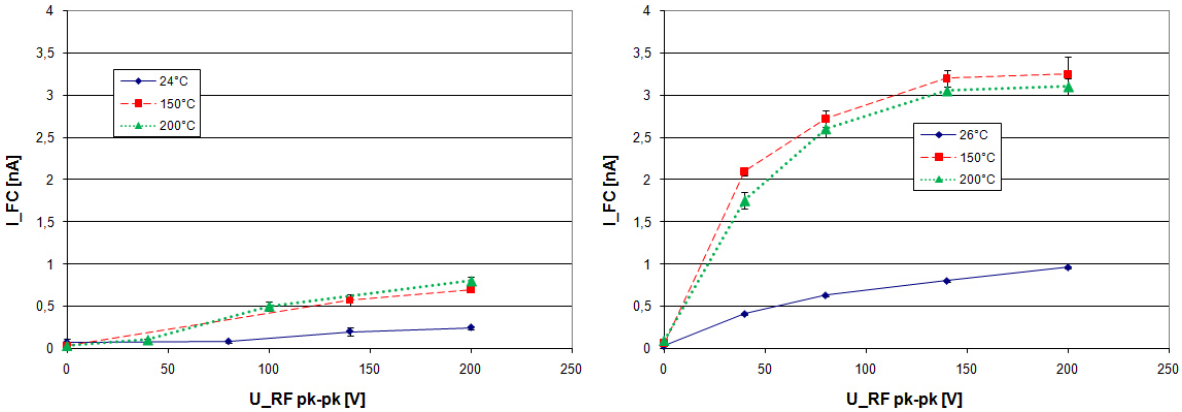

(a) 20mil ID 8.5cm capillary (b) 30mil ID 8.5cm capillary

Figure 6.8: Comparison between 8.5 cm long capillaries. (a) At least some current gets transmitted through the funnel (no transmission for longer 20mil capillaries). (b) Heating supports droplet evaporation and improves transmission by a factor of 3.

and re-condensation at the capillary walls is suspected to create large droplets instead of assisting droplet evaporation. The shorter length and the improved measurement through the Faraday cup extension demonstrate that the 20 mil capillary can be used, but works very inefficient in the used experimental setup compared to a 30 mil inner diameter capillary.

6.3.3 Differences between solute molecules

With improvements in gas flow and measurement setup the redesigned prototype is comparable to setups used by other research groups. Gly-Gln was compared to cytochrome c using the optimum parameters that are a temperature of 200 °C and a 8.5 cm long 30 mil capillary. First the

transmitted current was measured over frequency at a peak-to-peak RF voltage of 80 V and then the peak-to-peak RF voltage was increased at the best frequency to get the best possible transmission.

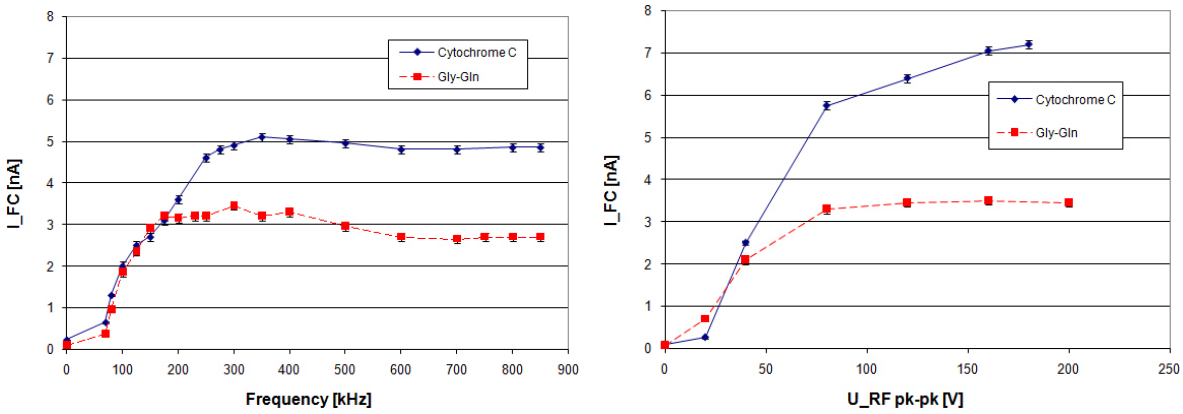

(a) Frequency spectrum (b) Amplitude spektrum at optimum frequency

Figure 6.9: Comparison between Gly-Gln and cytochrome c. The transmitted current is similar up to 230 kHz funnel frequency. Whereas the current using Gly-Gln (Mass: 203 u, charge state 1^+) does not increase for larger frequencies reaches cytochrome c current (Mass: 12500 u, charge state $11^+ - 24^+$) a saturation at about 300kHz and 5nA. With cytochrome c a remarkable transmission of 82 % is reached at $U_{pk-pk} = 150$ V

Figure 6.9 (a) shows the transmitted currents over frequency. Both currents are almost identical for frequencies under 180 kHz. For higher frequencies the transmitted current using Gly-Gln reaches a saturation at 3.2 nA whereas the current using cytochrome c reaches its saturation at a frequency of 350 kHz at 5 nA. For Gly-Gln the total maximum - talking figure 6.9 (b) into consideration - is reached at a current of 3.5 nA. This indicates strong space charge inside the ion funnel compared to cytochrome c. The heavier and higher charged cytochrome c ions result in a lower space charge and allow currents up to 7.2 nA or a transmission

of 82 %. This result exceeds comparable results from literature [14] where transmission up 60 % are reached.

This excellent result proves a proper design of the ion funnel and shows the influence of gas flow inside the first pumping stage. But it also reveals that the ion beam spreads out again after being focused through the ion funnel. The influences of gas flow and spreading out beam are investigated further in the next subsection.

6.3.4 Investigation of the effects of wrapping the funnel and extending the Faraday cup

Modifying the gas flow and extending the Faraday cup currents up to 7.2 nA could be transmitted through the ion funnel. The last experiment was done to get further understanding of the composition of the ions beam and the influence of modifying the gas flow.

The figures 6.10 and 6.11 show the coherence between wrapped and unwrapped funnel and regular and extended Faraday cup. If the funnel is unwrapped the shape of the graph is similar, but the intensity is a lot lower (top to bottom). If the Faraday cup is not extended, the former broad frequency response degrades to a narrower one and the intensity is lower (left to right).

This indicates that the ion beam consists of different size molecules/ droplets with different charge states and/or velocities. The ion funnel

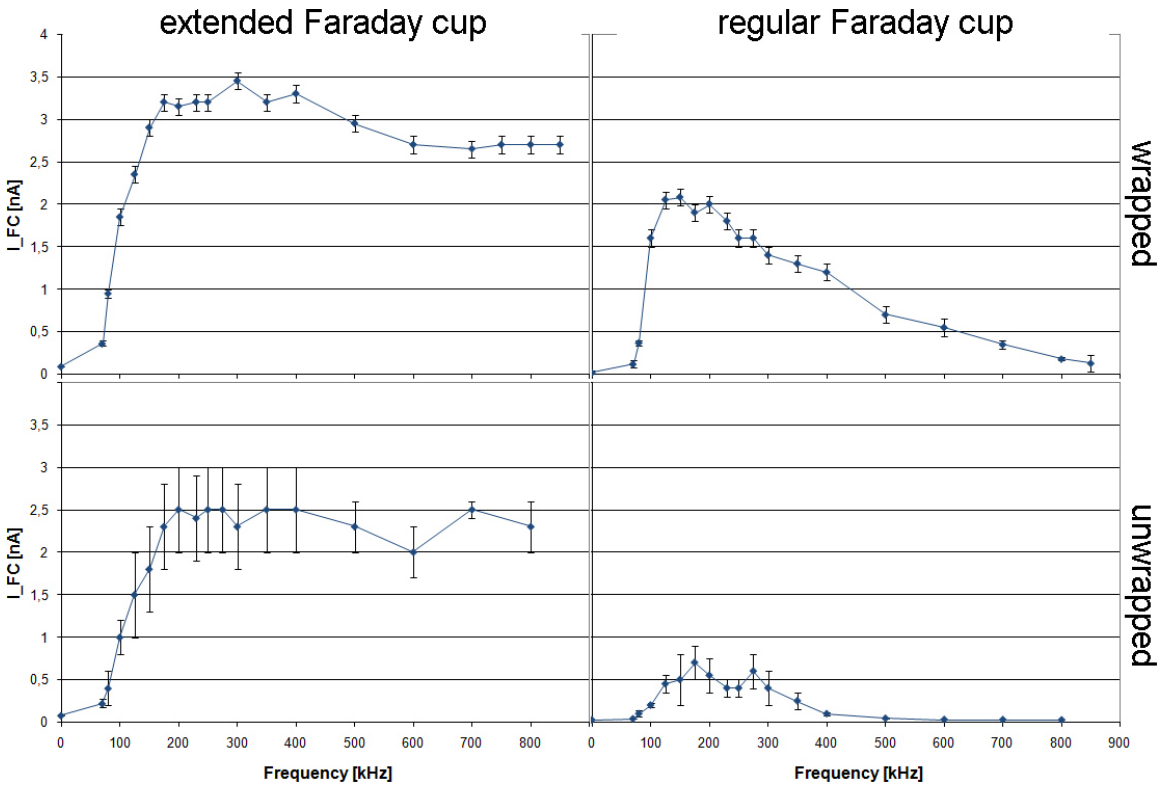

Figure 6.10: Effects of wrapping the funnel and extending the Faraday cup over funnel frequency. 0.5 mg/ml Gly-Gln in 50:50:1 methanol:water:acetic acid was sprayed at a temperature of 150 ℃ (DC gradient 18 V/cm, U_{pk-pk} 80 V, I_{Funnel} 6.6 − 8.2 nA). Top left: 52 % transmission at 300 kHz. Top right: narrow peak around 150 kHz, 25.5 % transmission. Bottom left: Same spectrum as top left, but only 31 % transmission. Bottom right: Similar graph to top right, but only 9 % transmission. This indicates a mass distribution of droplets/ions inside the funnel and frequency dependent transmission of the different masses.

transmits depending on the frequency not all of the charged particles, at least not a U_{pk-pk} of 80 V. Figure 6.9 shows that larger voltages increase the transmission. After the funnel exit the ion beam spreads out again, but the at lower funnel frequencies particels are transmitted through the funnel that spread out at a lower speed (higher current into Faraday cup) whereas at higher frequencies particles are transmitted that spread out

faster. If the funnel is not wrapped, the gas stream towards the pump exit affects all different particles equally which is indicated by the same shape of the graphs and the lower intensity of the unwrapped one.

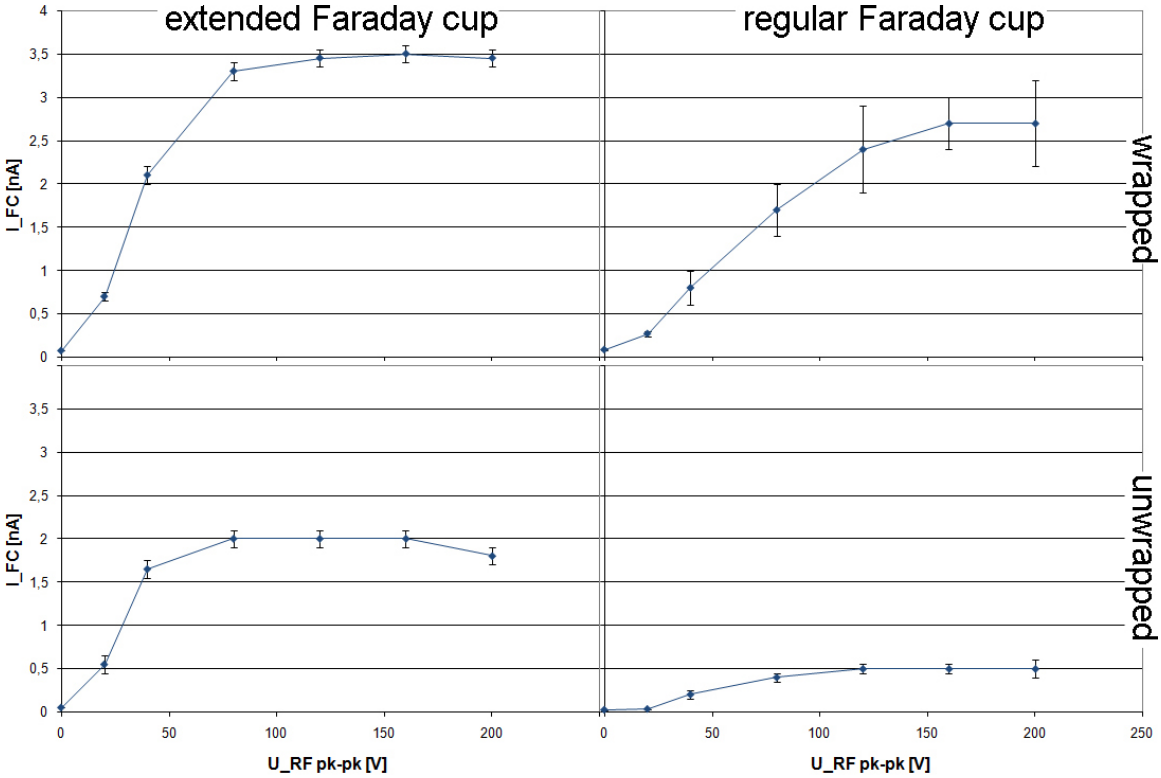

Figure 6.11: Effects of wrapping the funnel and extending the Faraday cup over funnel amplitude.

In figure 6.11 the experiment was repeated at the optimum frequencies for each case. The transmitted current over the amplitude confirm the results from the previous experiment. This experiment concludes the work for this thesis. The results build a stable base for further developments of the system. It is crucial for the next design phase to attach the quadrupole ion guide as close as possible to the ion funnel exit, because otherwise the beam will be spread out too far and additional loss occurs.

7 CONCLUSION

Previous to this work ion currents up to 930 pA could be transmitted through the ion funnel into the second pumping stage of the prototype system. The existing prototype system was thoroughly characterized and improvements were tried without major success. Problems in the droplet to ion evaporation process were assumed to be responsible for the low performance of the ion funnel. Heating the capillary using halogen lights was tried in combination with electrical heating on the vacuum side of the capillary to improve the droplet evaporation. Different capillary diameters and spray modes were tried, as well as parameter optimization in operation pressure and spray distance.

After a redesign phase the new prototype containing a new designed, improved ion funnel and a new capillary heater were commenced. After electrical checks of the funnel it was tried to find the best operating parameters for the system. It was tried to decrease the influence of the gas flow from the vacuum chamber inlet to the pump exit by wrapping the funnel into foil. Simulations of the gas flow were made. Transmission could be improved over a large frequency range comparable to other

publications. But though similar shaped graphs could be measured, the absolute values were not consistent with literature. Extending the Faraday cup to the exit orifice of the ion funnel solved this problem.

To conclude this work it is to mention that currents up to 7.2 nA could be transmitted through the ion funnel. A transmission efficiency of 82 % was reached modifying the air flow. Crucial for the ion funnel transmission efficiency is the droplet evaporation process. Nano-electrospray is necessary due to its high ionization efficiency and the resulting small droplet sizes. Uniform heating across the inlet capillary supports the droplet evaporation process and prevents condensation or frozen droplets. Together with the modified gas flow the heater is the most important element decreasing loss.

In the next design phase an ion guide will be designed. A quadrupole element can be used to focus, filter and guide the ions after the funnel exit into higher vacuum chambers. The higher mean free path in those regions simplifies ion optic design since known and established design methods can be used. Times in the region of one hour for depositing one monolayer across 1 cm^2 are possible. Multi-capillary/Multi-emitter ion sources could be used to improve the current into the vacuum chamber and decreasing deposition times further.

LIST OF REFERENCES

[1] M. E. Belov, M. V. Gorshkov, H. R. Udseth, G. A. Anderson, A. V. Tolmachev, D. C. Prior, R. Harkewicz, and R. D. Smith. Initial implementation of an electrodynamic ion funnel with fourier transform ion cyclotron resonance mass spectrometry. *Journal of the American Society for Mass Spectrometry*, 11(1):19–23, 2000.

[2] M. Cloupeau and B. Prunet-Foch. Electrostatic spraying of liquids in cone-jet mode. *Journal of Electrostatics*, 22(2):135–159, 1989.

[3] R. B. Cole. Some tenets pertaining to electrospray ionization mass spectrometry. *Journal of Mass Spectrometry*, 35(7):763–772, 2000.

[4] R. B. Cole and A. K. Harrata. Solvent effect on analyte charge state, signal intensity, and stability in negative ion electrospray mass spectrometry; implications for the mechanism of negative ion formation. *Journal of the American Society for Mass Spectrometry*, 4(7):546–556, 1993.

[5] M. Dole, R. L. Hines, L. L. Mack, R. C. Mobley, L. D. Ferguson, and M. B. Alice. Gas phase macroions. *Macromolecules*, 1(1):96–97, 1968.

[6] J. Fernandez de la Mora, J. Navascues, F. Fernandez, and J. Rosell-Llompart. Generation of submicron monodisperse aerosols in electrosprays. *J. Aerosol. Sci*, 21:5673–5676, 1990.

[7] J. Fernandez de la Mora, M. Labowsky, and J. B. Fenn. A continuum model for ion evaporation from a drop: effect of curvature and charge on ion solvation energy. *Analytica Chimica Acta*, 406(1):105–118, 2000.

[8] Dr Rudy Schlaf's Group Homepage. Electrospray thin film deposition of macro-molecular materials in vacuum [online]. [accessed 21st april 2008]. available from the world wide web: <http://rsl.eng.usf.edu/pages/researchelectrospray.html>, 04 2008.

[9] Dr Rudy Schlaf's Group Homepage. Moleculewriter [online]. [accessed 21st april 2008]. available from the world wide web: <http://rsl.eng.usf.edu/pages/researchmolwriter.html>, 04 2008.

[10] Anthony T. Iavarone, John C. Jurchen, and Evan R. Williams. Effects of solvent on the maximum charge state and charge state distribution of protein ions produced by electrospray ionization. *Journal of the American Society for Mass Spectrometry*, 11(11):976–985, 2000.

[11] R. R. Julian, S. R. Mabbett, and M. F. Jarrold. Ion funnels for the masses: Experiments and simulations with a simplified ion funnel. *Journal of the American Society for Mass Spectrometry*, 16(10): 1708–12, 2005.

[12] P. Kebarle and Y. Ho. Electrospray ionization mass spectrometry: Fundamentals, instrumentation and applications. pages 3–63. John Wiley & Sons: New York, 1997.

[13] P. Kebarle, D. B. Hager, N. J. Dovichi, and J. Klassen. Droplet electrospray mass spectrometry. *Analytical Chemistry*, 66(22):3944–3949, 1994.

[14] T. Kim, A. V. Tolmachev, R. Harkewicz, D. C. Prior, G. Anderson, H. R. Udseth, R. D. Smith, T. H. Bailey, S. Rakov, and J. H. Futrell. Design and implementation of a new electrodynamic ion funnel. *Anal. Chem*, 72(10):2247–2255, 2000.

[15] E. P. Kremer, G. J. Evans, and R. E. Jervis. A novel method for the collimation of ions at atmospheric pressure. *Journal of Physics D: Applied Physics*, 39(23):5008–5015, 2006.

[16] B. Lin and J. Sunner. Ion transport by viscous gas flow through capillaries. *Journal of the American Society for Mass Spectrometry*, 5:873–885, 1994.

[17] L. B. Loeb, A. F. Kip, and G. G. Hudson. Pulses in negative point-to-plane corona. *Physical Review*, 60(10):714–722, 1941.

[18] J. A. Loo. Studying noncovalent protein complexes by electrospray ionization mass spectrometry. *Mass Spectrometry Reviews*, 16(1): 1–23, 1997.

[19] J. A. Loo and R. R. O. Loo. Electrospray ionization mass spectrometry: Fundamentals, instrumentation and applications. pages 385–419. John Wiley & Sons: New York, 1997.

[20] Simon Papadopoulos, Klaus D. Jurgens, and Gerolf Gros. Protein diffusion in living skeletal muscle fibers: Dependence on protein size, fiber type, and contraction. *Biophys. J.*, 79(4):2084–2094, 2000.

[21] R. J. Pfeifer and C. D. Hendricks. Parametric studies of electrohydrodynamic spraying. *AIAA J*, 6:496–502, 1968.

[22] B. N. Pramanik, P. L. Bartner, U. A. Mirza, Y. H. Liu, and A. K. Ganguly. Electrospray ionization mass spectrometry for the study of non-covalent complexes: an emerging technology. *Journal of Mass Spectrometry*, 33(10):911–920, 1998.

[23] John William Strutt Lord Rayleigh. On the equilibrium of liquid conducting masses charged with electricity. *Phil. Mag.*, 14:184, 1882.

[24] R. Saf, T. E. Hamedinger, T. Steindl, J. Albering, and S. Rentenberger. Direct patterning of functional materials via atmospheric-pressure ion deposition. *2005 NSTI Nanotechnology Conference and Trade Show*, pages 467–470, 2005.

[25] Andrea Schmidt, Michael Karas, and Thomas Dülcks. Effect of different solution flow rates on analyte ion signals in nano-esi ms, or: when does esi turn into nano-esi? *Journal of the American Society for Mass Spectrometry*, 14(5):492–500, 2003.

[26] S. A. Shaffer, A. Tolmachev, D. C. Prior, G. A. Anderson, H. R. Udseth, and R. D. Smith. Characterization of an improved electrodynamic ion funnel interface for electrospray ionization mass spectrometry. *Anal. Chem.*, 71(15):2957–2964, 1999.

[27] A. P. Snyder, American Chemical Society Division of Analytical Chemistry, and American Chemical Society Meeting. *Biochemical and Biotechnological Applications of Electrospray Ionization Mass Spectrometry*. American Chemical Society, 1995.

[28] A Stark. *Performance Optimization of a 3D Patterning Device for Macro-Molecular Materials*. Studienarbeit, Ulm University, 2007.

[29] L. Tang and P. Kebarle. Effect of the conductivity of the electrosprayed solution on the electrospray current. factors determining analyte sensitivity in electrospray mass spectrometry. *Analytical Chemistry*, 63(23):2709–2715, 1991.

[30] L. Tang and P. Kebarle. Dependence of ion intensity in electrospray mass spectrometry on the concentration of the analytes in the electrosprayed solution. *Analytical Chemistry*, 65(24):3654–3668, 1993.

[31] G. I. Taylor. Disintegration of water drops in an electrical field. *Proc. R. Soc*, 280:383–397, 1964.

[32] G. J. Van Berkel. Electrospray ionization mass spectrometry: Fundamentals, instrumentation and applications. pages 65–105. John Wiley & Sons: New York, 1997.

[33] G. J. Van Berkel and F. Zhou. Characterization of an electrospray ion source as a controlled-current electrolytic cell. *Analytical Chemistry*, 67(17):2916–2923, 1995.

[34] G. Wang and R. B. Cole. *J. Am. Soc. Mass. Spectrom.*, 7:1050, 1996.

[35] M. Yamashita and J. B. Fenn. Electrospray ion source. another variation on the free-jet theme. *The Journal of Physical Chemistry*, 88(20):4451–4459, 1984.